NASA/TM-20240004230

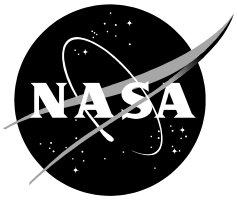

Experimental Results for Mars Rotorcraft Airfoils (roamx-0201 and clf5605) at Low Reynolds Number and Compressible Flow in a Mars Wind Tunnel

Witold J. F. Koning, Natalia Perez Perez, Haley V. Cummings
Ames Research Center, Moffett Field, California

Takayuki Nagata, Yudai Kanzaki, Miku Kasai, Muku Miyagi, Taku Nonomura, Keisuke Asai
Tohoku University, Sendai, Miyagi, Japan

Lidia Caros, Oliver Buxton, Peter Vincent
Imperial College London, London, England, United Kingdom

April 2024

NASA STI Program Report Series

The NASA STI Program collects, organizes, provides for archiving, and disseminates NASA's STI. The NASA STI program provides access to the NTRS Registered and its public interface, the NASA Technical Reports Server, thus providing one of the largest collections of aeronautical and space science STI in the world. Results are published in both non-NASA channels and by NASA in the NASA STI Report Series, which includes the following report types:

- TECHNICAL PUBLICATION. Reports of completed research or a major significant phase of research that present the results of NASA Programs and include extensive data or theoretical analysis. Includes compilations of significant scientific and technical data and information deemed to be of continuing reference value. NASA counterpart of peer-reviewed formal professional papers but has less stringent limitations on manuscript length and extent of graphic presentations.

- TECHNICAL MEMORANDUM. Scientific and technical findings that are preliminary or of specialized interest, e.g., quick release reports, working papers, and bibliographies that contain minimal annotation. Does not contain extensive analysis.

- CONTRACTOR REPORT. Scientific and technical findings by NASA-sponsored contractors and grantees.

- CONFERENCE PUBLICATION. Collected papers from scientific and technical conferences, symposia, seminars, or other meetings sponsored or co-sponsored by NASA.

- SPECIAL PUBLICATION. Scientific, technical, or historical information from NASA programs, projects, and missions, often concerned with subjects having substantial public interest.

- TECHNICAL TRANSLATION. English-language translations of foreign scientific and technical material pertinent to NASA's mission.

Specialized services also include organizing and publishing research results, distributing specialized research announcements and feeds, providing information desk and personal search support, and enabling data exchange services.

For more information about the NASA STI program, see the following:

- Access the NASA STI program home page at http://www.sti.nasa.gov

- Help desk contact information:

https://www.sti.nasa.gov/sti-contact-form/
and select the "General" help request type.

NASA/TM-20240004230

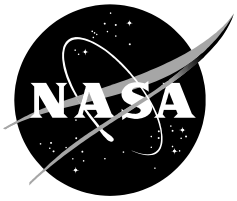

Experimental Results for Mars Rotorcraft Airfoils (roamx-0201 and clf5605) at Low Reynolds Number and Compressible Flow in a Mars Wind Tunnel

Witold J. F. Koning, Natalia Perez Perez, Haley V. Cummings
Ames Research Center, Moffett Field, California

Takayuki Nagata, Yudai Kanzaki, Miku Kasai, Muku Miyagi, Taku Nonomura, Keisuke Asai
Tohoku University, Sendai, Miyagi, Japan

Lidia Caros, Oliver Buxton, Peter Vincent
Imperial College London, London, England, United Kingdom

National Aeronautics and
Space Administration

Ames Research Center
Moffett Field, California 94035-1000

April 2024

ACKNOWLEDGMENTS

The research of Witold J. F. Koning, Natalia Perez Perez, and Haley Cummings is made possible by the NASA FY21 Space Technology Mission Directorate Early Career Initiative Project "Rotor Optimization for the Advancement of Mars eXploration." Thanks goes to Michael LaPointe and Richard Howard for their outstanding support and leadership. Peter Vincent has been supported by the Engineering and Physics Sciences Research Council, UK under awards EP/R030340/1 and EP/R029423/1. Takayuki Nagata, Yudai Kanzaki, Miku Kasai, and Taku Nonomura have been supported by the Japan Society for the Promotion of Science, KAKENHI under award JPJSBP120239906. Judith Carrodeguas, Nahri Ahn and Terry Pagan are thanked for their invaluable assistance in enacting the Space Act Agreement between NASA and Tohoku University, Japan, and NASA and Imperial College London, London, United Kingdom. Elderson Mercado Rivera, Eb Isaacs, Catherine Catrambone, and Sajon Seaberg are thanked for expertise in preparing the model geometries. Tove Ågren, Larry Young, and Sesi Kottapalli are thanked for their efforts in reviewing this document.

Many acknowledgments are in order for the ROAMX project. First to the Rotorcraft Aeromechanics Branch, and especially William Warmbrodt, Wayne Johnson, Larry Young, Ethan Romander, Tom Norman, Gloria Yamauchi, Carl Russel, Gina Willink, Alex Sheikman, Shirley Burek, Natasha Schatzman, Lauren Wagner, Shannah Withrow-Maser, Joshua Bowman, Kristen Kallstrom, Michelle Dominguez, Alyna Anderson, Alan Wadcock, Michael Radotich, and Raghuvir Singh – thank you for your support. Farid Haddad, J. (Bob) Balaram, Theodore Tzanetos, Benjamin Pipenberg, Anubhav Datta, Ravi Lumba, Cheng Chi, J. Ken Smith, Charles Cornelison, Alfredo Perez, Mani Ramasamy, Frank Pichay, David Hash, Peter Race, Scott Eddlemon, David Williams, Larry Hogle, Yvonne Desilva, Michael Boyd, Allison Bellows, Michael Derderian, Andrea Rosini, and Andrey Avramenko, thank you all for your support. Susan Gorton, thank you for your mentorship. Rosatina Chan, thank you for your support. Jay Fletcher, Samuel Montez, Chad Frost, William Van Dalsem, Jay Bookbinder, Harry Partridge, Penelope Boston, Debra Reiss-Bubenheim, Kayvon Sharghi, Mary Beth Wilhelm, and Sarah D'Souza, thank you for your support through the proposal writing process and beyond.

Available from:

NASA STI Support Services
Mail Stop 148
NASA Langley Research Center
Hampton, VA 23681-2199
757-864-9658

National Technical Information Service
5301 Shawnee Road
Alexandria, VA 22312
webmail@ntis.gov
703-605-6000

This report is also available in electronic form at

http://ntrs.nasa.gov

TABLE OF CONTENTS

LIST OF FIGURES

LIST OF TABLES

NOMENCLATURE

A, B	=	PSP calibration coefficients
b	=	span, m
c	=	chord, m
C_d	=	drag coefficient, $D/(0.5\rho V^2 S)$
C_l	=	lift coefficient, $L/(0.5\rho V^2 S)$
C_p	=	pressure coefficient, $(P-P_\infty)/(0.5\rho V^2 c)$
D	=	aerodynamic drag force, N
I	=	image intensity
L	=	aerodynamic lift force, N
M	=	Mach number
P	=	pressure, Pa
r	=	rotor radial coordinate, m
R	=	rotor radius, m
Re	=	chord-based Reynolds number, $\rho V c/\mu$
S	=	wing surface area, bc, m^2
t	=	airfoil ss, m
V	=	resultant velocity, m/s
x	=	streamwise coordinate, m
α	=	angle of attack, deg
ρ	=	test section gas density, kg/m^3
μ	=	dynamic viscosity, Ns/m^2

Subscripts

ref	=	reference condition
run	=	run condition
∞	=	freestream condition

Abbreviations

ARC	Ames Research Center
CFD	Computational Fluid Dynamics
CNC	Computer Numerical Control
DAQ	Data Acquisition
EDM	Electrical Discharge Machining
ELISA	Evolutionary aLgorithm for Iterative Studies of Aeromechanics
JPL	Jet Propulsion Laboratory
LSB	Laminar Separation Bubble
MH	Mars Helicopter
OML	Outer Mold Line
PAL	Planetary Aeolian Laboratory
PSP	Pressure Sensitive Paint
ROAMX	Rotor Optimization for the Advancement of Mars eXploration
SAA	Space Act Agreement

TS	Tollmien-Schlichting (waves)
UMD	University of Maryland

ABSTRACT

Experimental results are obtained for a roamx-0201 type airfoil and the clf5605 airfoil at high-subsonic, low Reynolds number conditions using the Tohoku University Mars Wind Tunnel, Japan. The tests are conducted at a Mach number of $M = 0.60$, and a Reynolds number of $Re = 20{,}000$ to reflect representative aerodynamics of a rotor blade for Mars exploration. The angle of attack is varied between $\alpha = -2.0$ deg and $\alpha = 6.0$ deg. The roamx-0201 type airfoil is an unconventional airfoil optimized for the chosen tunnel operating conditions using the Evolutionary aLgorithm for Iterative Studies of Aeromechanics (ELISA), developed under the Rotor Optimization for the Advancement of Mars eXploration (ROAMX) project. ELISA is utilized here to optimize aerodynamic airfoil performance using a Genetic Algorithm and two-dimensional high-fidelity CFD simulations, ultimately resulting in a Pareto-optimal airfoil set. The clf5605 airfoil is the outboard airfoil used on the Ingenuity Mars Helicopter and provides a baseline against which the roamx-0201, as well as possible future airfoil profiles for the compressible low Reynolds number regime, can be compared against. Lift and drag data are recorded using a balance, pressure distributions are obtained using Pressure Sensitive Paint (PSP) application, and Schlieren images are obtained to visualize the flowfield. The data is tabulated to aid future research.

INTRODUCTION

In April 2021, the Ingenuity Mars Helicopter made history as the first vehicle to demonstrate controlled, powered flight on another planet. In doing so, Ingenuity paved the way for future, more capable helicopters to conduct science and exploration on Mars and other planets (e.g. the future Mars rotorcraft proposed in Ref. [1]). This feat was the culmination of decades of research conducted at NASA Ames Research Center (ARC), Jet Propulsion Laboratory (JPL), Stanford University, Georgia Tech, University of Maryland (UMD), and others [2, 3, 4].

The Rotor Optimization for the Advancement of Mars eXploration (ROAMX) project is part of the efforts at ARC to conduct research in support of future rotorcraft on Mars [5]. ROAMX focuses on key aerodynamic rotor performance topics facing Mars rotorcraft. These topics include airfoil and rotor aerodynamic computational design and analysis specifically for the compressible, low-Reynolds number aerodynamic regime, and experimental validation of computational predictions. The Evolutionary aLgorithm for Iterative Studies of Aeromechanics (ELISA) software tool was developed in support of the ROAMX project [6]. ELISA was developed to enable aerodynamic airfoil and rotor hover optimization for low Reynolds number flows in the Mars atmosphere.

ELISA was utilized in the present work to optimize an unconventional roamx-0201 type airfoil [6, 7] for representative Mars atmospheric conditions ($Re = 20{,}000$ and $M = 0.60$)[1]. The clf5605 airfoil[2] [8], used on the outboard sections of the Ingenuity rotor, serves as a baseline to compare against the roamx-0201 [6, 7] profile. As existing research on airfoil and rotor aerodynamics at

[1] This Reynolds number and Mach number combination is consistent with Ingenuity class (~1.2-1.4m diameter) rotors. Other, larger, future Mars rotorcraft could operate outside this target Reynolds number, and ELISA, or similar tools, would have to be used to optimize for such new notional families of airfoils.

[2] The clf5605 airfoil was originally developed by AeroVironment, Inc. for terrestrial applications such as high-altitude long endurance UAV rotors/propellers and has been repurposed for Martian applications (Ingenuity).

high-subsonic, low Reynolds number conditions is notably limited in comparison to more conventional regimes, experimental validation of performance analyses, especially for unconventional airfoils, is necessary. The present work and on-going collaborations are setup to provide experimental and computational insights into airfoil performance at representative Mars conditions.

A Space Act Agreement (SAA) was set up with Tohoku University, Japan, to enable joint research on these airfoils utilizing the Tohoku University Mars Wind Tunnel in support of the ROAMX project and future Mars rotorcraft development, in general. The Mars Wind Tunnel at Tohoku University is unique in that it is a low-density tunnel that can simulate Martian atmospheric flight conditions [9, 10]. In addition to the Tohoku University and NASA ROAMX team, the Imperial College, London, was also brought in through a second SAA, and its researchers were also team members on this international effort involving three partners.

The goal of this work is to present the experimental setup and results from the airfoil performance testing performed at the Tohoku University Mars Wind Tunnel for the clf5605 and roamx-0201 type airfoils to enable future correlation efforts at these conditions for conventional airfoils (cambered tear-drop shaped) and unconventional airfoils (sharp-edged flat-plates with multiple camber inflection points).

First, the background of the research is presented together with the details of both experimental airfoil profiles. The experimental apparatus and data processing approach is discussed afterwards, followed by the results and concluding remarks. The tabulated mean lift and drag coefficients as obtained from the force measurements are presented in Appendix A, followed by the tabulated mean pressure distributions in Appendix B.

BACKGROUND

Before the launch of Ingenuity, research had been performed at ARC to computationally study Ingenuity's low-Reynolds number rotor performance in the Mars atmosphere, including rotor performance differences when the outboard airfoils were substituted for flat and cambered plates. The low density of the Mars atmosphere and the low temperature result in relatively unexplored high-subsonic low Reynolds number flows for rotor blade airfoils operating under those conditions. Early results had shown an improvement in rotor hover figure of merit, without any optimization of the profiles (a simple 1% t/c cambered plate with 5% camber at 0.50c) [11]. The result was of particular interest since no rotor or airfoil optimization was performed at the time. Even though the performance benefits of cambered plates were already indicated in limited research available on low Reynolds numbers, the predicted performance increase was achieved using a single airfoil geometry as a direct substitute for Ingenuity's outboard rotor airfoil.[3]

These results led to dedicated efforts to investigate airfoil optimization for unconventional profiles [12, 13] and further investigation of practical ways to accurately simulate flows in this aerodynamic regime [14]. The former presented challenges as convenient airfoil parameterization

[3] Cambered flat plate airfoils were suggested for Mars rotorcraft application as early as the 2000's, e.g., Ref. [37], though little computational or experimental substantiation was provided at the time.

for unconventional airfoils was not readily available, while the latter complicated optimization due to the costly nature of such computational analyses.

The unconventional airfoil profiles achieve their performance benefits by inducing immediate separation of the (laminar) boundary layer at the leading edge, followed by a shear layer instability that results in the shedding of large-scale vortices downstream which can lead to reattachment of the separated shear layer in the mean flow (consistent with 'flapping'-type bubbles [14]). Reattachment of the flow is of interest at very low Reynolds numbers since laminar separation is the primary impediment to airfoil performance at these conditions, while at typical (higher) Reynolds numbers one would generally prefer to avoid a Laminar Separation Bubble (LSB) in favor of on-body transition to a turbulent boundary layer. The separated shear layer instability is not dependent on amplification of small-scale disturbances, referred to as Tollmien-Schlichting (TS) waves, and thus presents a way to achieve reattachment of the separated shear layer in the low Reynolds number regime. This is especially noteworthy since the very low Reynolds numbers generally experienced in the Mars atmosphere make it progressively less likely one can rely on sufficient amplification of TS waves to cause reattachment; experimental on-body transition is usually not reported below Re = 100,000 [14, 15].

The unsteady flows experienced by unconventional airfoils in this transitional regime present several challenges to efficient airfoil computational analysis as turbulence at these conditions is hard to model - or resolve - and can be highly dependent on operating conditions and other catalysts to disturbance growth. Furthermore, the flows can be chaotic and therefore require that a relatively large number of flow passes be simulated before meaningful time-averages of the integrated aerodynamic coefficients can be obtained.

Only a portion of the ROAMX project's focus is on computational and experimental airfoil optimization and characterization. In parallel efforts with the airfoil work, the other principal focus of the ROAMX project is currently underway to investigate experimental rotor performance at Mars atmospheric conditions at ARC for the ELISA derived airfoils. The ARC Planetary Aeolian Laboratory (PAL) is a large vacuum chamber that allows for testing at Mars atmospheric densities. Several test campaigns were over several years were conducted by NASA Ames to investigate rotor performance and experimental complexity at very low densities [16, 17].

Early Mars rotor testing efforts were key to the launch of the STMD-funded Early Career Initiative ROAMX project to investigate the impact of optimization on both airfoils and rotors for operation on Mars, and the possible improvements in rotor performance [5]. ELISA was developed under ROAMX and was used to optimize the roamx-0201 geometry for the present work [6]. To be able to validate the airfoil performance studies, an SAA was established with Tohoku University, Japan, to allow for experimental testing of the cfl5605 and roamx-0201 type airfoils using force and pressure measurements and Schlieren imaging to capture the flow fields. Target conditions were chosen to be representative for rotor operation in the Mars atmosphere: Re = 20,000, M = 0.60, at which an angle of attack sweep from $\alpha = -2.0$ to $\alpha = 6.0$ deg was performed. A second SAA was set up with Imperial College London, England, to further enable collaboration and facilitate a second set of independent computational analyses using Direct Numerical Simulations (DNS) in PyFR [18, 19, 20].

EXPERIMENTAL AIRFOIL PROFILES

The Ingenuity rotor uses the 5% thick clf5605 profile outboard of $r/R = 0.50$ and shows significant chord planform variation with span in the outboard region. The original clf5605 airfoil profile used to create the Ingenuity rotor blade outer mold line (OML) was linearly thickened from leading to trailing edge to achieve a practical trailing edge thickness and resulted in a 0.5 mm thick trailing edge along the blade span [8].

The experimental airfoil-section test model for the clf5605 wind tunnel testing was based on the original airfoil profiles (prior to thickness modification) and adapted to use a 0.25%*c*-thick semicircular TE (as used in Ref. [21]) to stay as close as possible to the nominal profile, as shown in Figure 1.

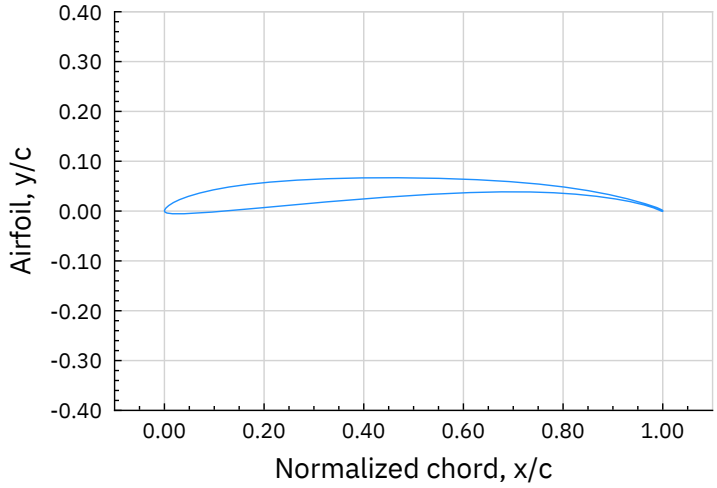

Figure 1. The clf5605 airfoil profile ($t/c = 0.05$).

The 1% thick roamx-0201 type airfoil [7, 1], as shown in Figure 2, followed from an airfoil optimization effort using the ELISA optimization framework. The airfoil was optimized for $Re = 20{,}000$, $M = 0.60$, which are approximate conditions at $r/R = 0.75$ for the ROAMX rotor [6]. The roamx-0201 parameterization (quadratic camber variation, constant thickness) is explained in more detail in Ref. [6] and was used here with a 1% baseline thickness and 5/1000 inch as the smallest radii for the leading and trailing edges.

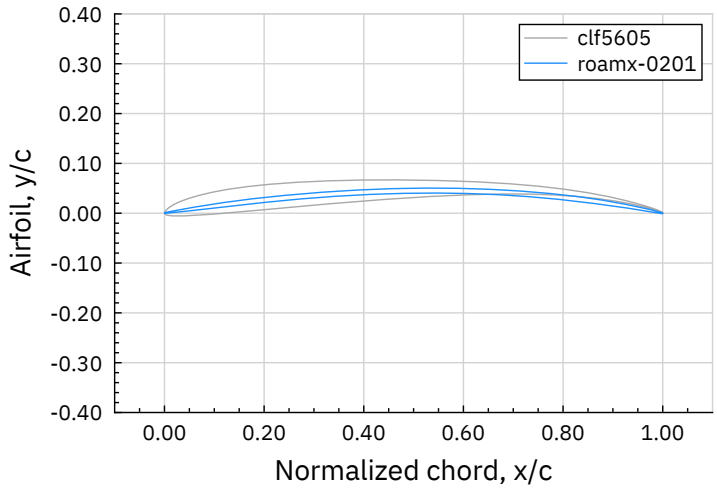

Figure 2. The roamx-0201 optimized airfoil profile (t/c = 0.01) and clf5605 airfoil (t/c = 0.05).

The optimized roamx-0201 geometry was selected from the Pareto optimal airfoil set (function of section lift and drag) to represent the peak sectional lift-to-drag ratio of around L/D = 26.0 at an angle of attack of around α = 4.48 deg. The airfoil geometry corresponding to peak lift-to-drag ratio was chosen to demonstrate the upper bound of airfoil performance of the roamx-0201 parametrization at these conditions. Future detailed airfoil design would need to include stall margin, likely lowering practical airfoil efficiency.

The resulting maximum camber was 4.55%c at a chordwise location of 0.538c, which is close to the 'classic' cambered plate model used in earlier work [11]. It is noted that optimization for different radial locations did result in deviation from this geometry, as shown in Ref. [6]. The profiles shown in Figure 1 and Figure 2 were used to manufacture the airfoil models in this report.

EXPERIMENTAL APPARATUS

Wind tunnel

The Tohoku University Mars Wind Tunnel [9, 10] was used. This wind tunnel is housed in a vacuum chamber as shown in Figure 3, and wind tunnel experiments can be conducted under low-pressure conditions. Various fundamental studies of compressible low-Reynolds-number flow over an airfoil [22, 23], plate [24, 25], and circular cylinder [26] have been conducted previously by Tohoku researchers, prior to the reported joint ROAMX airfoil study. Also, surface flow visualization for a small rotor blade using the pressure-sensitive paint and sublimation method has been conducted [27] by Tohoku University, independently of NASA's efforts to develop a next generation Mars rotorcraft beyond Ingenuity. The wind tunnel is driven by an ejector system [28], due to the inability of a fan to generate high-subsonic flow under low pressure conditions. The ejector system is located downstream of the test section and induces a flow in the wind tunnel by injecting a supersonic jet flow downstream of the measurement section. The pressure in the chamber increases due to the operation of the ejector. Therefore, an appropriate amount of gas is exhausted into a separately installed buffer tank, and the total pressure inside the wind tunnel can be maintained for a finite period. The amount of exhaust gas is adjusted by a PID-controlled butterfly valve installed in the flow path connecting the main tank and buffer tank. Figure 4 shows

the schematic of the test section. The test section of the wind tunnel is 100 mm wide and 150 mm in height. The upper and lower walls in the test section are inclined at an angle of 1.3 deg on each side. The inclination angle was determined by assuming a flat-plate laminar boundary layer at $P = 1$ kPa and $T = 288$ K using air as the driving gas.

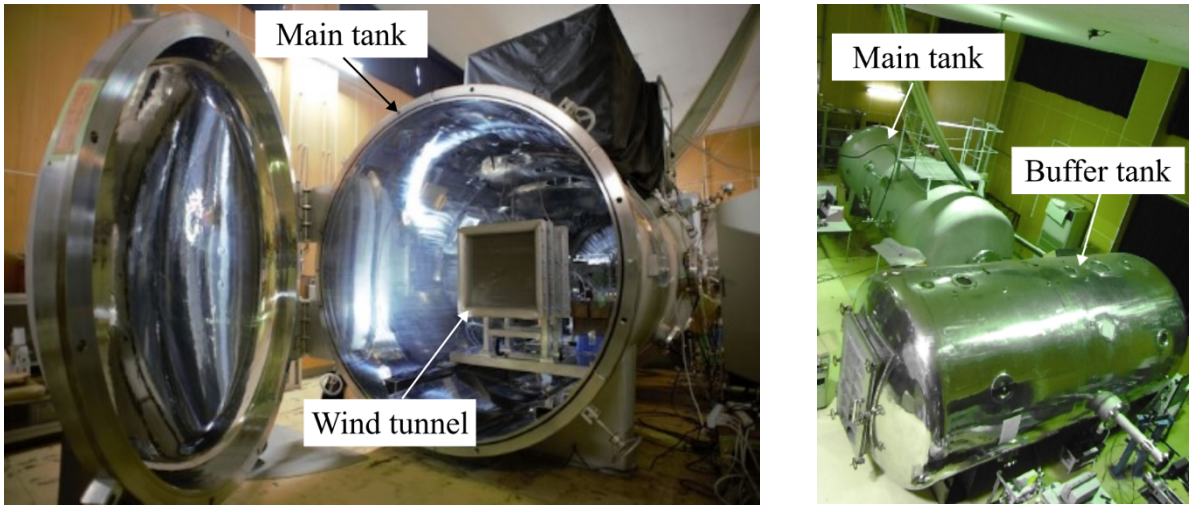

(a) Main tank and wind tunnel (b) Panoramic view

Figure 3. Tohoku University Mars wind tunnel.

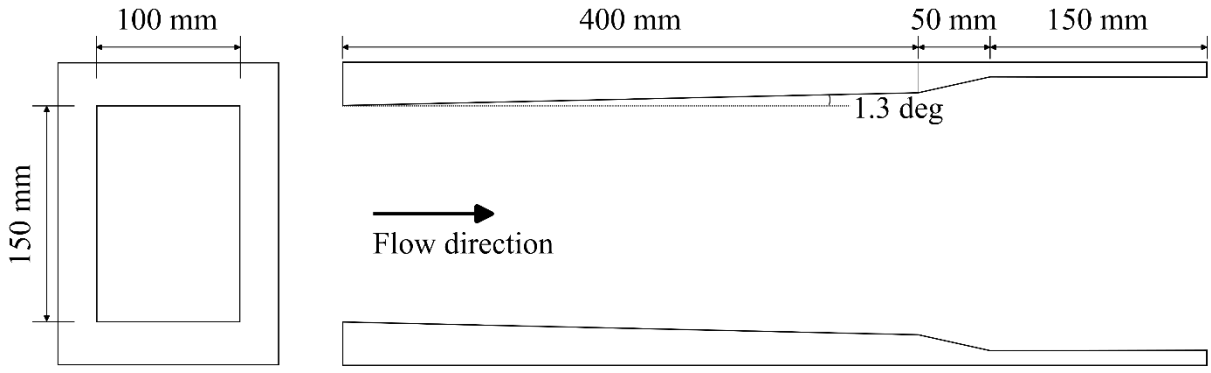

(a) Front view (b) Side view

Figure 4. Schematic of Tohoku University Mars wind tunnel test section.

Airfoil models

Table 1 lists all airfoil models that were fabricated. In total three models of the clf5605 profile and five models of the roamx-0201 profile were produced. For the clf5605 profile, models clf5605-us-s and clf5605-us-fp were fabricated in the United States from AISI 4130 using an Electrical Discharge Machining (EDM) method and used for Schlieren measurements, and force and PSP measurements, respectively, and model clf5605-jp-f was fabricated in Japan from A5052 using an EDM method and used for force measurements.

For the roamx-0201 profile, models roamx-0201-us-f, roamx-0201-us-pu, and roamx-0201-us-pl where fabricated in the United States from AISI 4130 using a Computer Numerical Control (CNC) mill and used for force measurements, upper surface PSP measurements, and lower surface PSP measurements, respectively. The roamx-0201-jp-s, and roamx-0201-jp-fp models were fabricated in Japan from A5052 using an EDM method and used for Schlieren measurements, and force and PSP measurements, respectively. All models were manufactured to have a span $b = 99.7$ mm and chord $c = 50$ mm. Models roamx-0201-us-f, roamx-0201-us-pu, and roamx-0201-us-pl were slightly thicker than the target roamx-0201 profile due to manufacturing limitations (the intended chord length for these airfoils on the ROAMX rotor is around $c = 100$ mm). Similarly, all models of the clf5606 profile likely have trailing edges that are slightly too thick relative to the target profile. Future data analysis and computational work will look to quantify the impact of these profile deviations on overall airfoil lift/drag characteristics. Figure 5 shows the side profile of the clf5606-us-s model. In addition, the surface texture also differs depending on the model. The roamx-0201-us models have machining marks due to the CNC milling process. The models fabricated in Japan have slightly rougher surfaces than those fabricated in the United States. This is because, unlike the models fabricated in the United States, the models fabricated in Japan did not undergo a polishing process after EDM processing. Omitting this polishing step allows for a very thin and sharp profile, which improves profile reproducibility.

Figure 5. Side profile ($c = 50$mm) of the cfl5605 profile after EDM (clf5605-us-s).

Table 1. List of test models.

Base Profile	Manufacturing Method	Measurement	Material	Model Designation
clf5605	EDM	Schlieren	AISI 4130	clf5605-us-s
		Force and PSP	AISI 4130	clf5605-us-fp
	EDM	Force	A5052	clf5605-jp-f
roamx-0201	CNC mill	Force	AISI 4130	roamx-0201-us-f
		PSP (upper side)	AISI 4130	roamx-0201-us-pu
		PSP (lower side)	AISI 4130	roamx-0201-us-pl
	EDM	Schlieren	A5052	roamx-0201-jp-s
		Force and PSP	A5052	roamx-0201-jp-fp

The clf5605-us-fp model, shown in Figure 6a, uses a pressure tap on the upper and lower surface of the airfoil for pressure calibration during PSP measurements. The pressure taps are routed out to the side of the airfoil profile to facilitate connection to the pressure gages. The roamx-0201-us-pu and roamx-0201-us-pl models are too thin to route the pressure tap within the profile, and

therefore use a through-hole, and a thin tube on the opposite side of the airfoil is used to obtain the reference pressure data. This naturally requires separate measurements for the upper and lower sides.

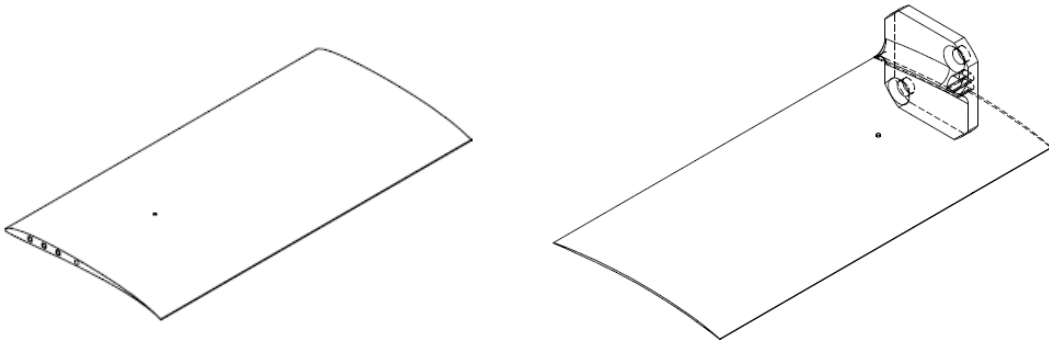

(a) clf5605-us-fp model for PSP (b) roamx-0201-us-pu model for PSP

Figure 6. Schematics of airfoil models for PSP measurements.

The roamx-0201 based PSP models require separate models for upper and lower sides since the mounting bracket is part of the assembly, as shown in Figure 6b, and hence the model cannot be reversed to illuminate the lower surface. This contrasts with clf5605 based PSP models which have sufficient thickness to fix the mounting bracket with screws, see Figure 6a. The roamx-0201-jp-fp model was initially only intended for force measurements but was later also used for upper surface PSP measurements.

Experimental setup

The setup for Schlieren visualization is shown in Figure 7. The Schlieren optical system uses a white LED (PFBR-600SW-LL, CCS) as a light source. A pinhole (F70, Surugaseiki) with a diameter of 2.0 mm was used and a point light source was created. A concave mirror with a focal length of 1500 mm was used as the first and second collimators, and a plano-convex lens with a focal length of 1000 mm was used as the imaging lens. The knife edge was installed horizontally, and the lower half of the light flux was cutoff at the focal point of the second collimator, which visualized the density gradient field perpendicular to the freestream. The time-series Schlieren images were taken by high-speed camera (SA-X2, Photoron). The exposure time and frame rate were 2.5 μs and 72,000 fps, respectively. In this experiment, parallel light was reflected by a plane mirror and passed through the test section due to space constraints in the laboratory. The airfoil model was mounted directly between the optical glasses of the wind tunnel side wall, as shown in Figure 8. The influence of noise caused by atmospheric fluctuations was reduced physically by covering the optical path with duct hoses both outside and inside the main tank, as shown in Figure 9.

The lift and drag forces were measured using a three-component force balance system. This balance system consists of load cells (LC-4100-G-600 and LC-4101-K-003, A&D) for drag and lift directions and a stepping motor (PK513PA-H50S, Oriental Motor LTD) for adjusting the angle of attack. The accuracy of the stepping motor is 0.0144 deg. The zero angle of attack was determined by the inclinometer, and an airfoil mold was used for placing the inclinometer on the airfoil to ensure a reliable reference surface. The accuracy of the mold placement onto the airfoil was not quantified. However, it is noted that the roamx-0201-us models were slightly altered by

the machining process and gaps between the mold and airfoil model were observed. The accuracy of the inclinometer used to determine a 0-degree pitch angle is 0.1 deg.

The rated capacity of the load cell for the drag and lift directions are 6 N and 30 N, respectively, and the accuracies are 0.9×10^{-3} N and 4.5×10^{-3} N, respectively. The forces and other quantities used for calculating aerodynamic force coefficients were recorded by a Data Acquisition (DAQ) system (PCI6251, National Instruments) with a sampling frequency of 10 Hz.

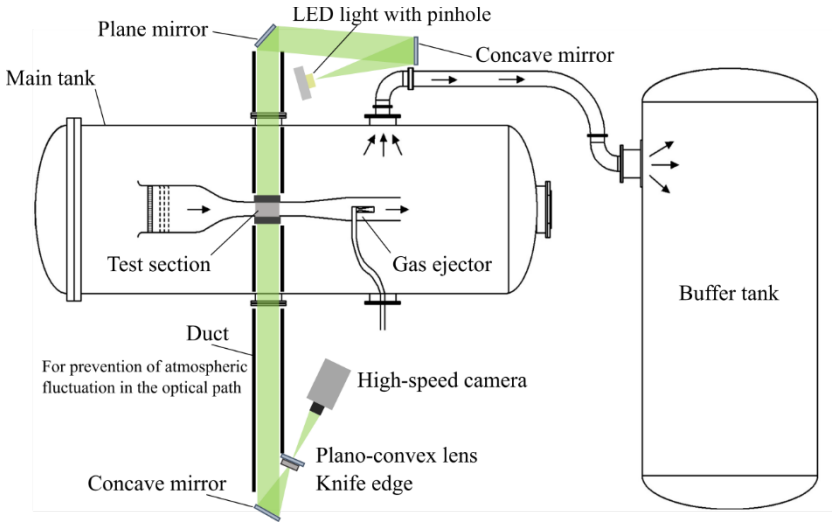

Figure 7. Schematic diagram of optical system for Schlieren visualization.

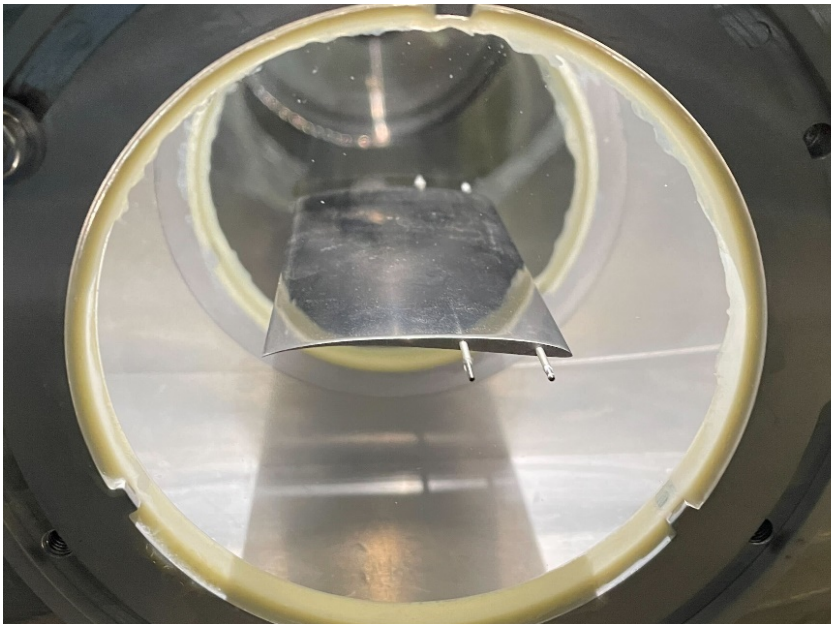

Figure 8. Schlieren setup with the clf5605-us-s model mounted between the optical glass.

(a) Inside the main tank (b) Outside the main tank

Figure 9. Duct for the light path.

Single-point unsteady pressure measurements and planar steady pressure measurements were performed. The unsteady pressure measurement was conducted by the pressure transducer (CCQ-093-5A, Kulite Semiconductor Products). Time-resolved pressure measurements on the upper and lower surfaces were carried out as individual experiments. The signal from the unsteady pressure sensor was amplified by an amplifier (570ST, TEAC). The signals were recorded by a data logger (WE7000, Yokogawa) with a sampling frequency of 10 Hz.

The planar steady pressure measurements were performed by polymer-based PSP [29]. Under low-pressure conditions, the normalized sensitivity which is normalized by the ambient pressure and time response of PSPs is generally degraded [30, 31, 32]. Therefore, PSP specialized for the low-pressure condition should be used. The PSP used in the present study was composed of Pd(II) meso-tetra(pentafluorophenyl) porphyrin (PdTFPP) luminophore and poly [1-(trimethylsilyl)-1-propyne] [poly(TMSP)] polymer [33], which has high sensitivity to pressure under low-pressure conditions [34, 35]. Although polymer-based PSPs for unsteady measurement under low-pressure conditions [36] have been developed recently, the present study was focused on the time-averaged pressure measurement.

Figure 10 and Figure 11 show a schematic diagram of the experimental setup of the PSP measurement and photograph of PSP optical system and a PSP-coated model. Two UV-LEDs (IL-106, Hardsoft) were used as an excitation light, and an S-CMOS camera (C13440-20CU, Hamamatsu Photonics) was used as a photo detector. A camera lens (Nikkor 105 mm f/2.0, Nikon) was used as an imaging lens with a band-pass filter (640 ± 50 nm) to cutoff the light other than PSP emission. Excitation of PSP and imaging of PSP emission were carried out through the optical windows of the main tank and upper wall of the wind tunnel. The optical system was covered with a blackout curtain to prevent stray light. Exposure time for the imaging was set between 20–200 ms so that the image intensity becomes approximately 80% of the full well-capacity of the image sensor. The wind-on, reference and dark-current images were acquired. The number of images obtained was 100 for each image, and random noise was reduced by taking the average for each image set.

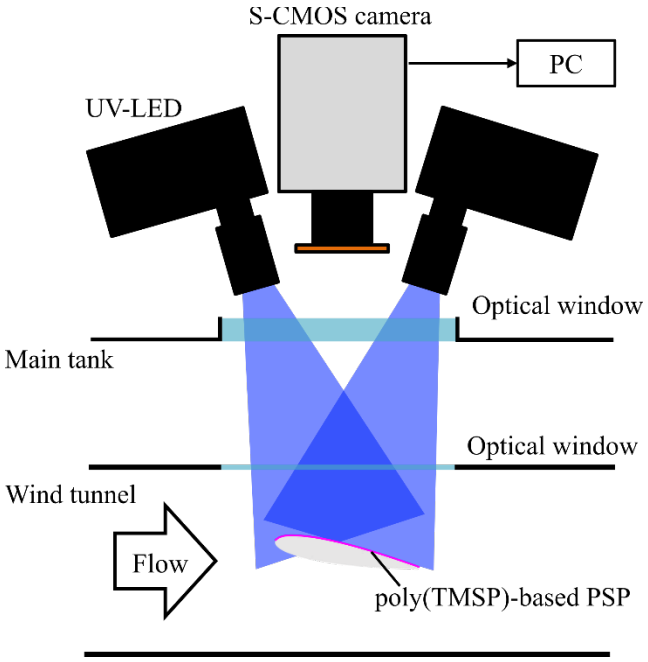

Figure 10. Schematic of optical system for PSP measurement.

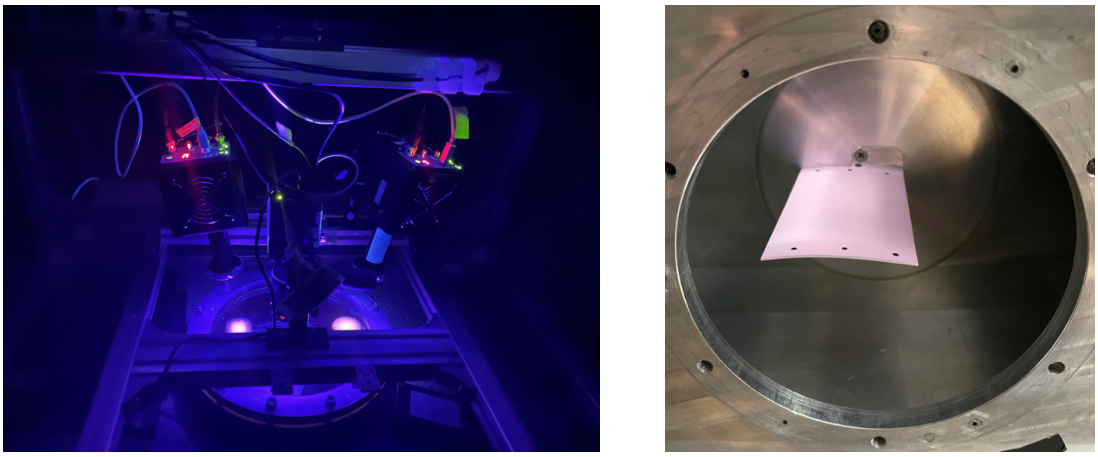

(a) Optical system for PSP measurement (b) roamx-0201-us-pu PSP model

Figure 11. Experimental setup for PSP measurement.

The Stern–Volmer coefficient and the temperature sensitivity of the PSP used in the present experiment were approximately 0.78 and −1.41%/K, respectively, at the ambient pressure of 10 kPa and the temperature of 283 K. Note that the Stern–Volmer coefficient of the PSP can be degraded due to photodegradation, and the lowest value in the present experiment was approximately 0.6. The PC-PSP binder of [37] with a reduced particle mass content of 85 wt% without the luminophore was used as the white base coat. PSPs using poly(TMSP) polymers have a contamination issue due to oil mist from the vacuum pump, resulting in a run-to-run variation in pressure sensitivity distribution. To account for this variability, calibration tests were conducted in the wind tunnel before every execution. The pressure in the main tank was changed for seven

conditions, and the sensitivity distribution was obtained by correlating the pressure and intensity of the PSP emission at each pressure.

The target flow condition was $M = 0.6$ at $Re = 20{,}000$, and the angle of attack was varied from $\alpha = -2.0$ to $\alpha = 6.0$ deg. The conditions at which Schlieren visualization and PSP measurements were conducted were fewer in number compared to force measurement for practical reasons, as shown in Table 2.

Table 2. List of experimental conditions.

α [deg]	Schlieren visualization	Force measurement	PSP measurement
−2.0	×	×	×
0.0	×	×	×
2.0	×	×	×
2.5		×	
3.0	×	×	×
3.5		×	
4.0	×	×	×
4.5		×	
5.0	×	×	×
5.5		×	
6.0	×	×	×

DATA PROCESSING

The Reynolds and Mach numbers and other quantities used to obtain aerodynamic force coefficients were calculated based on the wind tunnel data recorded at 10 Hz. Averages were obtained over a period of six seconds (24,000 flow passes), during which the Reynolds and Mach number remained approximately constant.

Schlieren visualization

All Schlieren images displayed in the present report are raw images with simple contrast enhancement. Image quality can be improved by de-noising via band-pass filtering and/or singular value decomposition-based approaches [38]. Such de-noising processing might be performed in future work.

Force measurement

Time-averaged forces and associated standard deviations were calculated. The data length used for calculation was six seconds, during which the Reynolds and Mach number remained approximately constant. Average output of the balance system under the wind-off condition immediately before starting each run was subtracted from the time-series force data.

PSP measurement

Figure 12 shows the image processing procedure for PSP images. The averaged dark current image was subtracted from the averaged reference and wind-on images. The pressure was calculated based on the normalized Stern–Volmer equation, which is normalized by the reference (wind-off) condition, as follows:

$$\frac{I_{\mathrm{ref}}}{I} = \alpha\left(A + B\frac{P}{P_{\mathrm{ref}}}\right)$$

where A and B are the calibration coefficients which are determined by the calibration test. Although the intensity of the PSP emission can also depend on temperature, the temperature distribution was not measured. In the present study, the influence of the temperature distribution on the obtained pressure distribution was reduced by using the wind-off image acquired immediately after execution as a reference image. In addition, the pressure distribution obtained by PSP was adjusted using a correction factor α determined to ensure consistent pressure measurements from the pressure tap and those obtained by PSP around the pressure tap.

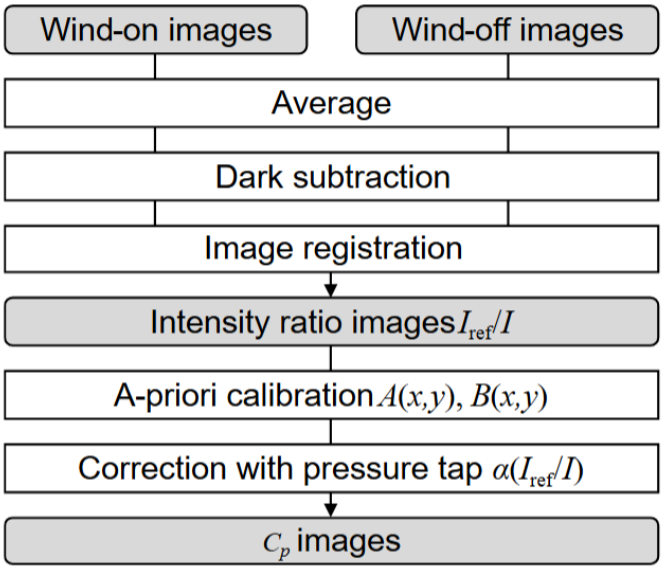

Figure 12. Flow chart of image processing for PSP images.

RESULTS

Schlieren visualization

Table 3 presents the actual flow conditions at which the Schlieren visualization was performed for the clf5605-us-s model. Figure 13 shows the corresponding instantaneous Schlieren images. At $\alpha = -2.0$ and 0.0 deg, the flow on the lower side is separated at the leading edge. Although the angle of attack is negative or zero, flow separation occurs on the upper side. As the angle of attack increases, the flow separation tends to occur closer to the leading edge, and a strong separated shear layer is generated from the trailing edge on the lower side.

Table 3. Operating conditions in Schlieren visualization over the clf5605-us-s model.

α [deg]	Re	M
−2.0	19,766	0.588
0.0	19,948	0.598
2.0	19,984	0.601
3.0	20,070	0.605
4.0	20,055	0.603
5.0	19,959	0.601
6.0	19,952	0.599

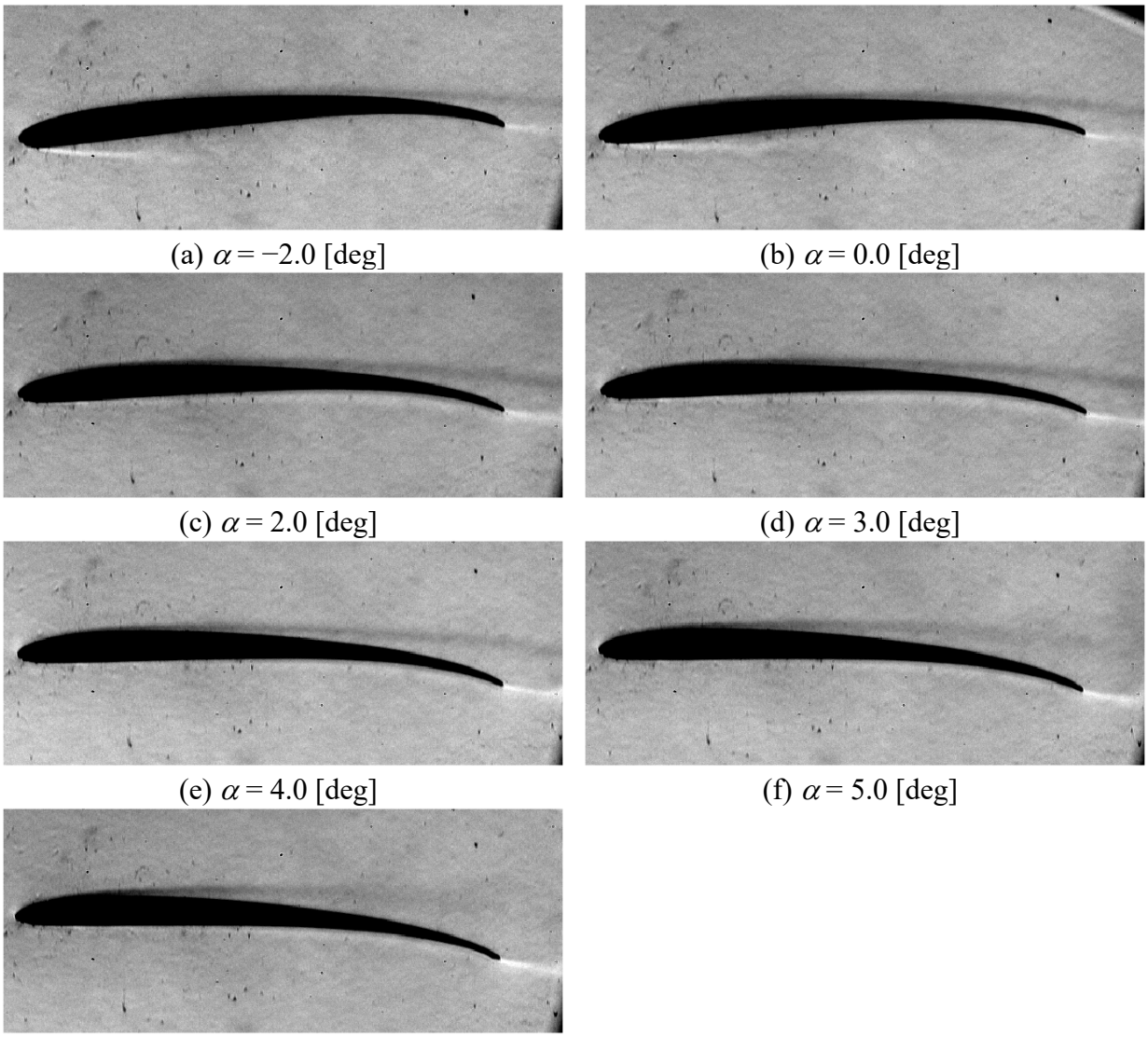

(a) $\alpha = -2.0$ [deg] (b) $\alpha = 0.0$ [deg]

(c) $\alpha = 2.0$ [deg] (d) $\alpha = 3.0$ [deg]

(e) $\alpha = 4.0$ [deg] (f) $\alpha = 5.0$ [deg]

(g) $\alpha = 6.0$ [deg]

Figure 13. Instantaneous Schlieren images of flow over the clf5605-us-s model.

Table 4 presents the actual flow conditions at which the Schlieren visualization was performed for the roamx-0201-jp-s profile. Figure 14 shows the corresponding instantaneous Schlieren images.

For the clf5605 profile, flow separation occurs on the lower side at $\alpha = -2.0$ and 0.0 deg, and the separation point moves upstream as the angle of attack increases. The separation point identified from the Schlieren image is located around 50%*c* for $\alpha = 5.0$ deg for the roamx-0201-jp-s profile (compared to around ~20-25%c for the clf5605-us-s model). At $\alpha = 6.0$ deg, flow separates at the leading edge of the airfoil, and the generated separated shear layer reattaches on the surface around 50%*c*.

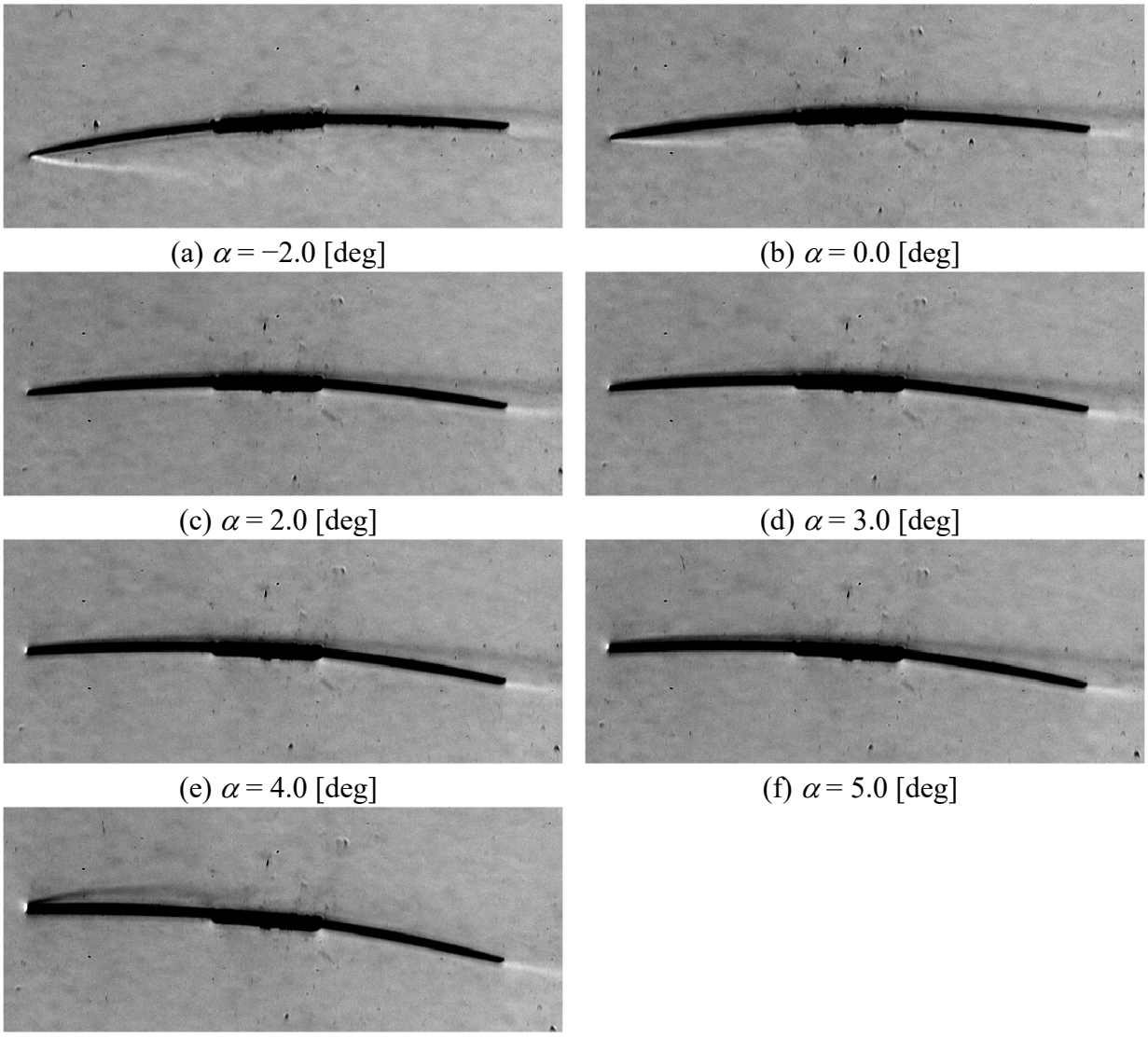

(a) $\alpha = -2.0$ [deg] (b) $\alpha = 0.0$ [deg]

(c) $\alpha = 2.0$ [deg] (d) $\alpha = 3.0$ [deg]

(e) $\alpha = 4.0$ [deg] (f) $\alpha = 5.0$ [deg]

(g) $\alpha = 6.0$ [deg]

Figure 14. Instantaneous Schlieren images of flow over the roamx-0201-jp-s profile.

Table 4. Operating conditions in Schlieren visualization over the roamx-0201-jp-s profile.

α [deg]	*Re*	*M*
−2.0	20,109	0.600
0.0	20,078	0.603
2.0	19,906	0.601
3.0	19,794	0.599
4.0	19,801	0.599
5.0	19,865	0.603
6.0	19,539	0.589

Force measurement

APPENDIX A lists the lift and drag coefficients and the actual Reynolds and Mach numbers for each condition. The standard deviation of the lift and drag coefficients were based on the variation in time of the aerodynamic forces.

Figure 15 and Figure 16 show the comparison of the lift and drag curves, respectively. Measurements at α = 0.0 deg and α = 6.0 deg were performed twice, to confirm repeatability. The shaded area represents the standard deviation range for each drag and lift coefficient. The obtained lift and drag curves differ between the clf5605-us-fp and clf5605-jp-f models, despite both models nominally being based on the same geometry. Similarly, the roamx-0201-us-f and roamx-0201-jp-fp models show differences in obtained lift and drag despite nominally being based on the same geometry.

The lift coefficient of the clf5605 based profiles is generally higher than that of the roamx-0201 based profiles, for equal angle of attack. The drag coefficient for the roamx-0201 based profiles is generally lower that then clf5605 based profiles, for equal angle of attack.

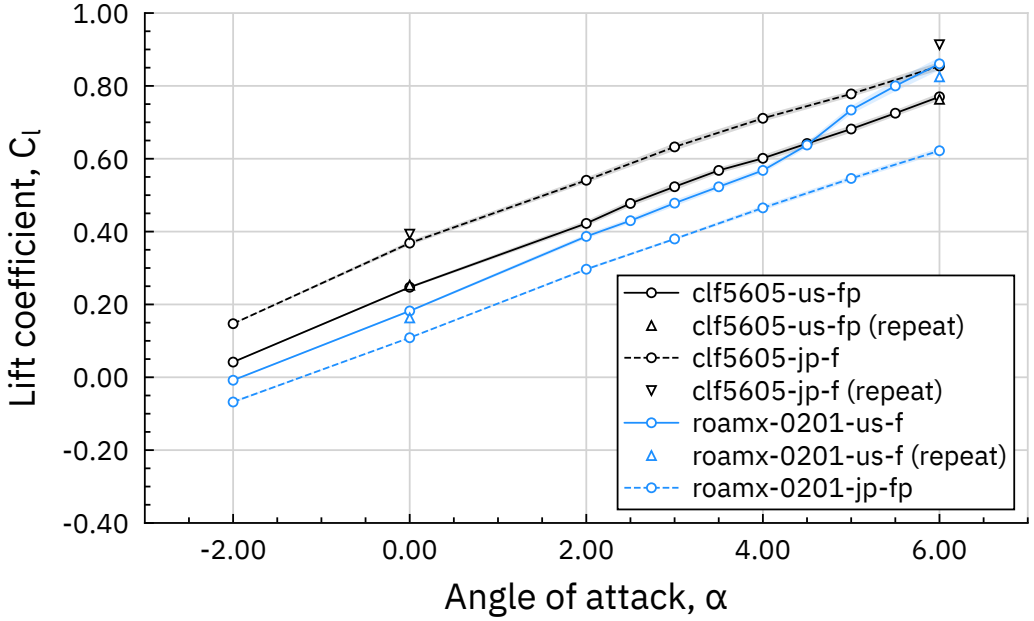

Figure 15. Comparison of lift curves.

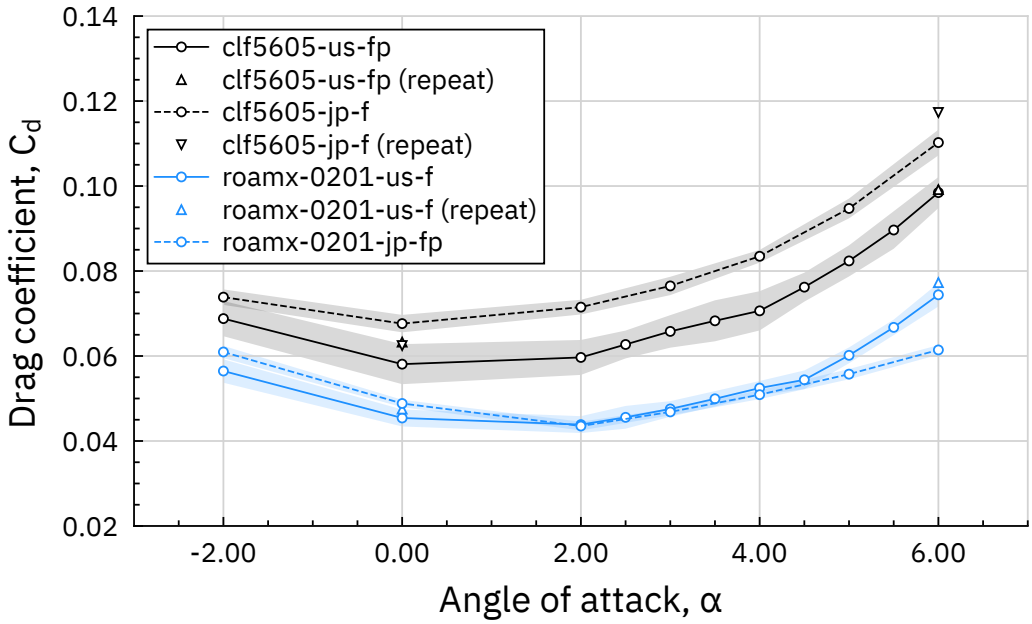

Figure 16. Comparison of drag curves.

Figure 17 and Figure 18 show the lift-to-drag ratios versus angle of attack and the drag polars, respectively. The drag polars remove the dependency of the data on angle of attack, and slightly improve the unification of the two profiles, possibly alluding to an offset in reference angle of attack as mentioned in the experimental setup chapter.

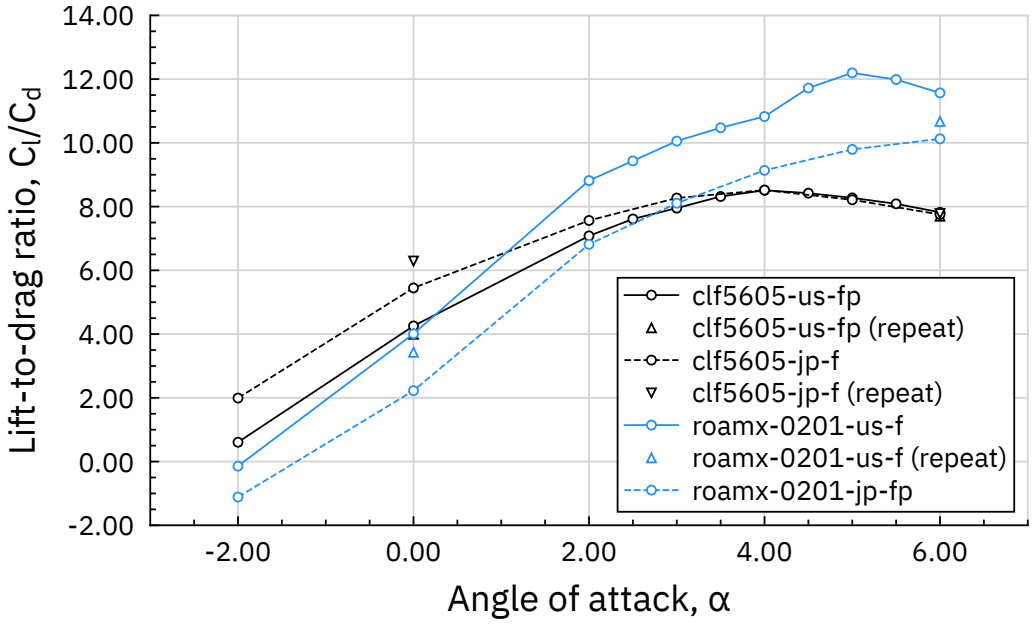

Figure 17. Comparison of lift-to-drag ratio curves.

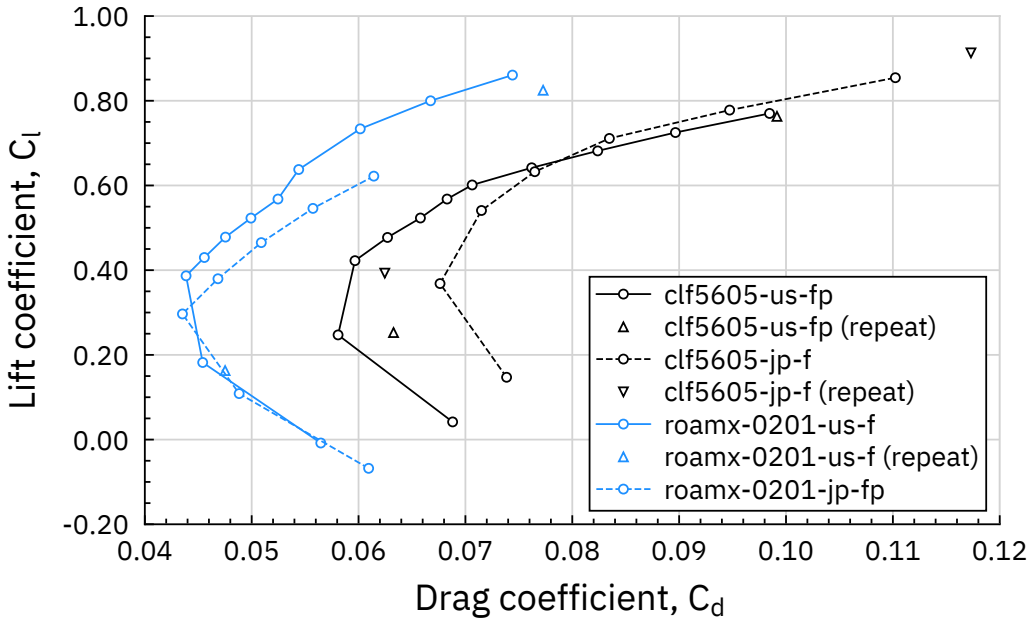

Figure 18. Comparison of drag polars.

PSP measurement

APPENDIX B tabulates the actual flow conditions and mean pressure distributions from the PSP measurements for the clf5605-us-fp, roamx-0201-us-pu, roamx-0201-us-pl and roamx-0201-jp-fp (upper side only) models. The corresponding pressure distributions at the model centerlines are shown in Figure 19 through Figure 21. Here, the C_p profiles were obtained by taking a spanwise average with a 5% span width (80 pixels) around the model centerline. The solid and dashed lines indicate the upper and lower surface pressure distributions, respectively. The difference between the C_p profile of the clf5605-us-fp and roamx-0201-us-pu (and roamx-0201-us-pl) can be primarily seen around the leading edge. First, the suction peak of the roamx-0201-us-pu and roamx-0201-us-pl is stronger and sharper than that of the clf5605-us-fp because of the sharper leading edge. Second, the pressure plateau region is formed at $\alpha = 6.0$ deg, consistent with the Schlieren images. Although the basic characteristics are similar to the roamx-0201-us-pu and roamx-0201-us-pl, the negative pressure on the leading-edge side of the roamx-0201-jp-fp is weaker than that of the roamx-0201-us-pu and roamx-0201-us-pl. This difference results in the lower C_l of the roamx-0201-jp-fp. However, the clf5605-us-fp pressure distributions show signs of trailing edge flow separation for the majority of angles of attack. Note that location mismatch due to airfoil deformation, self-illumination (only for lower side) or temperature variation possibly introduces an error in the C_p estimates.

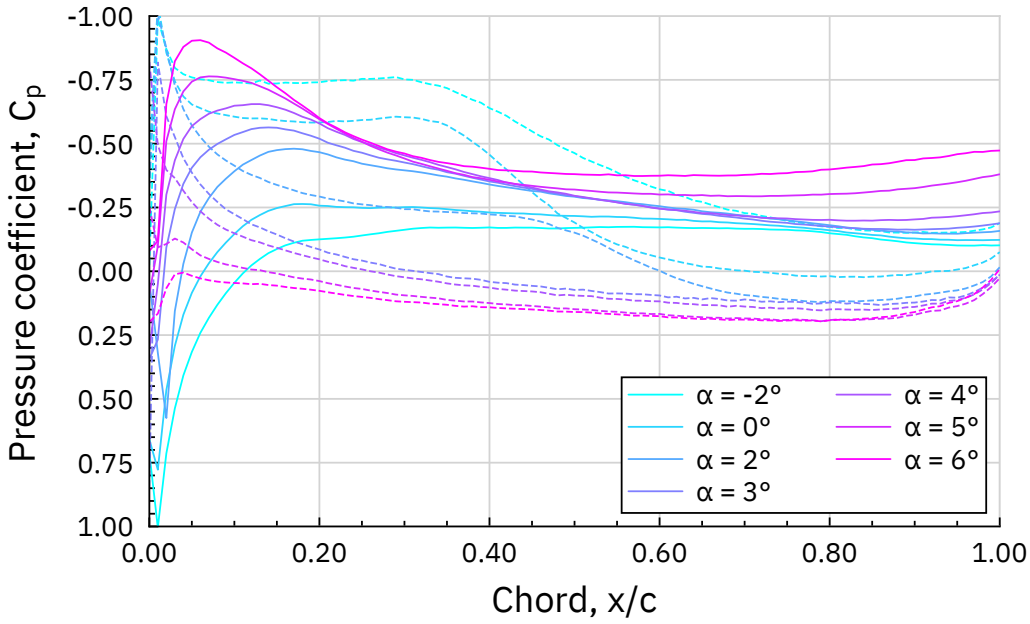

Figure 19. C_p chordwise distribution of clf5605-us-fp model (solid lines represent upper surface pressure).

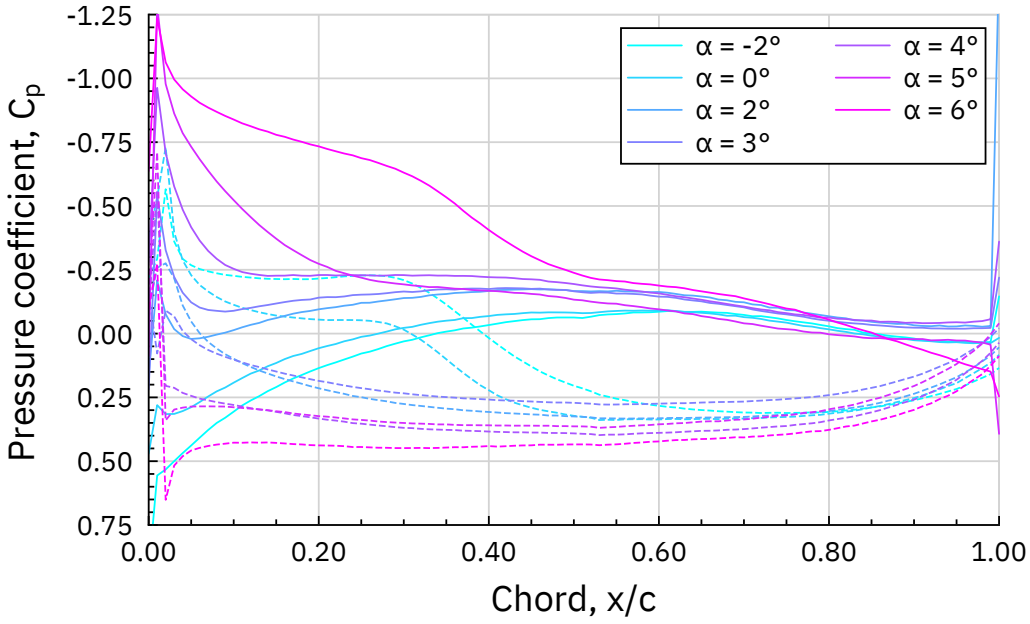

Figure 20. C_p chordwise distribution of roamx-0201-us-pu and roamx-0201-us-pl models (solid lines represent upper surface pressure).

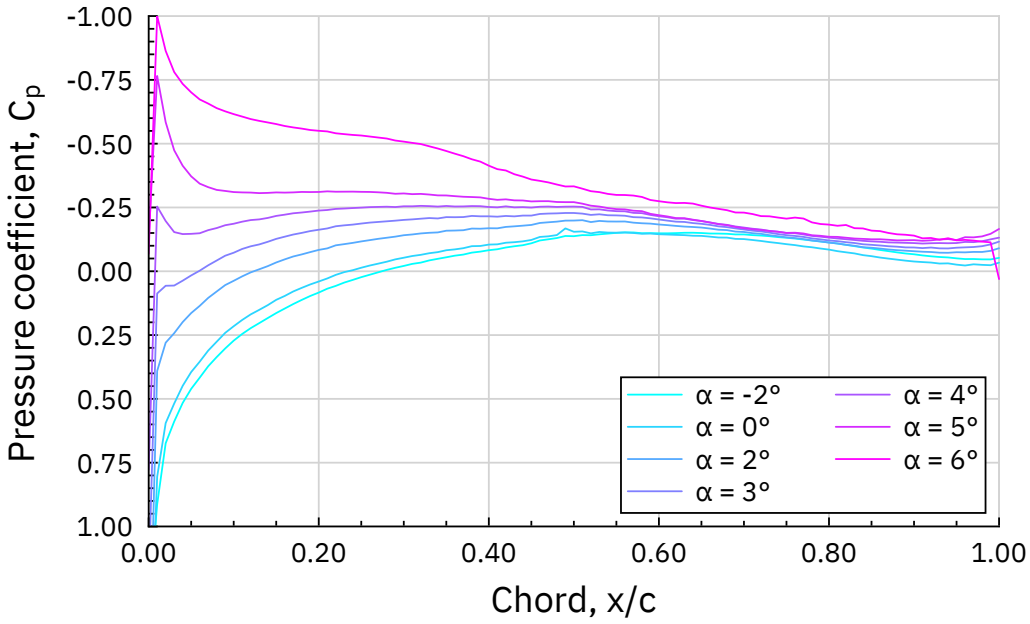

Figure 21. C_p chordwise distribution of roamx-0201-jp-fp (upper side only).

CONCLUDING REMARKS

Wind tunnel tests were performed in the Tohoku Mars Wind Tunnel, Japan, to evaluate the performance of the clf5605 airfoil (used for the Ingenuity Mars Helicopter rotors) and the relatively new roamx-0201 airfoil (potentially to be used for future Mars rotorcraft) at Mars atmospheric conditions (Re = 20,000 and M = 0.60). This was a joint test campaign between NASA, Tohoku University, and Imperial College London. The overall ongoing ROAMX effort, of which the airfoil wind tunnel test campaign was one part, is being led by NASA Ames Research Center, under funding provided by the NASA Space Technology Mission Directorate's (STMD) Early Career Initiative program. This wind tunnel airfoil testing reflects a significant expansion of the understanding of compressible low-Reynolds number airfoils, particularly those suitable for Mars rotorcraft rotors. For each airfoil, two models were fabricated using different manufacturing techniques, and force measurements, Schlieren images, and pressure measurements were obtained. It was observed that different models of the same airfoil led to different results - highlighting the difficulties around manufacturing limitations, and the challenges associated with obtaining data at low Reynolds number compressible conditions. Wind tunnel data corrections were not applied. The data is tabulated to serve as reference data for future research.

REFERENCES

[1] W. Johnson, S. Withrow-Maser, L. Young, C. Malpica, W. J. F. Koning, W. Kuang, M. Fehler, A. Tuano, A. Chan, A. Datta, C. Chi, R. Lumba, D. Escobar, J. Balaram, T. Tzanetos and H. Grip, "Mars Science Helicopter Conceptual Design," NASA/TM-2020-220485, Ames Research Center, Moffett Field, CA, 2020.

[2] J. Balaram, M. Aung and M. P. Golombek, "The Ingenuity Helicopter on the Perseverance Rover," *Space Science Reviews,* vol. 217, no. 56, 2021.

[3] G. K. Yamauchi, "A Summary of NASA Rotary Wing Research: Circa 2008–2018," NASA/TP—2019–220459, Ames Research Center, Moffett Field, CA.

[4] L. A. Young, M. R. Derby, R. Demblewski and J. Navarrete, "Experimental Investigation and Demonstration of Rotary-Wing Technologies for Flight in the Atmosphere of Mars," 58th Annual Forum of the American Helicopter Society, Montreal, Canada, 2002.

[5] H. Cummings, B. N. Perez Perez, W. J. F. Koning, W. Johnson, L. A. Young, F. Haddad, E. Romander, J. Balaram, T. Tzanetos, J. Bowman, L. Wagner, S. Withrow-Maser, E. Isaacs, S. Toney and Shirazi, "Overview and Introduction of the Rotor Optimization for the Advancement of Mars eXploration (ROAMX) Project," Aeromechanics for Advanced Vertical Flight Technical Meeting, Transformative Vertical Flight 2022, San Jose, CA, 2022.

[6] W. J. F. Koning, B. N. Perez Perez, H. V. Cummings, E. A. Romander and W. Johnson, "ELISA: A Tool for Optimization of Rotor Hover Performance at Low Reynolds Number in the Mars Atmosphere," VFS 6th Decennial Aeromechanics Specialists' Conference, Santa Clara, CA, 2024.

[7] W. J. F. Koning, B. N. Perez Perez and H. Cummings, "Preliminary Airfoil Design for Low Reynolds Numbers," NASA/TM-2022-6782, Ames Research Center, Moffet Field, CA, 2022.

[8] W. J. F. Koning and M. Dominguez, "Mars Helicopter Ingenuity Rotor Geometry," NASA/TM-20240001510, Ames Research Center, Moffett Field, CA, 2024.

[9] M. Anyoji, K. Nose, S. Ida, D. Numata, H. Nagai and K. Asai, "Development of a Low-Density Wind Tunnel for Simulating Martian Atmospheric Flight," *Transactions of The Japan Society for Aeronautical and Space Sciences,* vol. 9, 2011.

[10] M. Anyoji, S. Ida, K. Nose, D. Numata, H. Nagai and K. Asai, "Characteristics of the Mars Wind Tunnel at Tohoku University in CO2 Operation Mode," 48th AIAA Aerospace Sciences Meeting Including the New Horizons Forum and Aerospace Exposition, Orlando, FL, 2010.

[11] W. J. F. Koning, E. A. Romander and W. Johnson, "Low Reynolds Number Airfoil Evaluation for the Mars Helicopter Rotor," 74th Annual Forum of the American Helicopter Society, Phoenix, AZ, 2018.

[12] W. J. F. Koning, "Airfoil Selection for Mars Rotor Applications," NASA/CR—2019–220236, Ames Research Center, Moffett Field, CA, 2019.

[13] W. J. F. Koning, E. A. Romander and W. Johnson, "Optimization of Low Reynolds Number Airfoils for Martian Rotor Applications Using an Evolutionary Algorithm," in AIAA Scitech 2020 Forum, Orlando, FL, 2020.

[14] W. J. F. Koning, E. A. Romander, H. V. Cummings, B. N. Perez Perez and P. G. Buning, "On Improved Understanding of Airfoil Performance Evaluation Methods at Low Reynolds Numbers," *Journal of Aircraft,* vol. 60, no. 3, 2023.

[15] J. McMasters and M. Henderson, "Low-speed Single-element Airfoil Synthesis," *Technical Soaring,* vol. 6, no. 2, 1980.

[16] B. N. Perez Perez, G. A. Ament and W. J. F. Koning, "Experimental Forward Flight Rotor Performance Testing from Terrestrial to Martian Atmospheric Densities," NASA/CR-2019-220229, Ames Research Center, Moffet Field, CA, 2019.

[17] G. A. Ament, W. J. F. Koning and N. B. Perez Perez, "Isolated Rotor Forward Flight Testing at Martian Atmospheric Density Data Report," NASA/CR-2018-219736, Ames Research Center, Moffett Field, CA, 2018.

[18] L. Caros, O. Buxton, T. Shigeta, T. Nagata, T. Nonomura, K. Asai and P. Vincent, "Direct Numerical Simulation of Flow over a Triangular Airfoil Under Martian Conditions," *AIAA Journal,* vol. 60, no. 7, 2022.

[19] L. Caros, O. Buxton and P. Vincent, "Optimization of Triangular Airfoils for Martian Helicopters Using Direct Numerical Simulations," *AIAA Journal,* vol. 61, no. 11, 2023.

[20] F. D. Witherden, A. M. Farrington and P. E. Vincent, "PyFR: An open source framework for solving advection–diffusion type problems on streaming architectures using the flux reconstruction approach," *Computer Physics Communications,* vol. 185, no. 11, pp. 3028-3040, 2014.

[21] W. J. F. Koning, W. Johnson and H. F. Grip, "Improved Mars Helicopter Aerodynamic Rotor Model for Comprehensive Analyses," *AIAA Journal,* vol. 57, no. 9, 2019.

[22] P. M. Munday, K. Taira, T. Suwa, D. Numata and K. Asai, "Nonlinear lift on a triangular airfoil in low-Reynolds-number compressible flow," *Journal of Aircraft,* vol. 52, no. 3, pp. 924-931, 2015.

[23] M. Anyoji, D. Numata, H. Nagai and K. Asai, "Effects of Mach number and specific heat ratio on low-Reynolds-number airfoil flows," *AIAA Journal,* vol. 53, no. 6, pp. 1640-1654, 2015.

[24] É. Mangeol, D. Ishiwaki, N. Wallisky, K. Asai and T. Nonomura, "Compressibility effects on flat-plates with serrated leading-edges at a low Reynolds number," *Experiments in Fluids,* vol. 58, pp. 1-15, 2017.

[25] A. Guilarte Herrero, A. Noguchi, K. Kusama, T. Shigeta, T. Nagata, T. Nonomura and K. Asai, "Effects of compressibility and Reynolds number on the aerodynamics of a simplified corrugated airfoil," *Experiments in Fluids,* vol. 62, pp. 1-20, 2021.

[26] T. Nagata, A. Noguchi, K. Kusama, T. Nonomura, A. Komuro, A. Ando and K. Asai, "Experimental investigation on compressible flow over a circular cylinder at Reynolds number of between 1000 and 5000," *Journal of Fluid Mechanics,* vol. 893, p. A13, 2020.

[27] T. Nagata, H. Sato, M. Okochi, T. Matsuyama, Y. Sugioka, M. Kasai, K. Kusama, D. Numatam, T. Nonomura and K. Asai, "Visualization of pressure and skin-fiction fields on rotating blade under low-pressure conditions," *AIAA Journal,* vol. 60, no. 9, pp. 5422-5435, 2022.

[28] M. Anyoji, D. Numata, H. Nagai and K. Asai, "Supersonic Ejector-Driving System under Low Pressure: A Performance Evaluation," *Transactions of The Japan Society for Aeronautical and Space Sciences,* vol. 64, no. 3, pp. 156-164, 2021.

[29] T. Liu, J. P. Sullivan, K. Asai, C. Klein and Y. Egami, *Pressure and Temperature Sensitive Paint*s, Springer, Berlin, 2021.

[30] T. Nagata, M. Kasai, T. Okudera, H. Sato, T. Nonomura and K. Asai, "Optimum pressure range evaluation toward aerodynamic measurements using PSP in low-pressure conditions," *Measurement Science and Technology,* vol. 31, p. 085303, 2020.

[31] M. Kasai, D. Sasaki, T. Nagata, T. Nonomura and K. Asai, "Frequency response of pressure-sensitive paints under low-pressure conditions," *Sensors,* vol. 21, no. 9, p. 3187, 2021.

[32] M. Kasai, T. Nagata and T. Nonomura, "Indexes for evaluation of dynamic characteristics of pressure-sensitive paint based on pressure sensitivity and frequency response," *Measurement Science and Technology,* vol. 35, p. 065101, 2024.

[33] K. Nagai, T. Masuda, T. Nakagawa, B. D. Freeman and I. Pinnau, "Poly [1-(trimethylsilyl)-1-propyne] and related polymers: synthesis, properties and functions," *Progress in Polymer Science,* vol. 26, no. 5, pp. 721-798, 2001.

[34] H. Mori, T. Niimi, M. Hirako and H. Uenishi, "Pressure sensitive paint suitable to high Knudsen number regime," *Measurement Science and Technology,* vol. 17, no. 6, p. 1242, 2006.

[35] M. Anyoji, D. Numata, H. Nagai and K. Asai, "Pressure-sensitive paint technique for surface pressure measurements in a low-density wind tunnel," *Journal of Visualization,* vol. 18, no. 2, pp. 297-309, 2015.

[36] M. Kasai, T. Nagata, K. Uchida, T. Nonomura, K. Asai and Y. Egami, "Evaluation of characteristics of fast-response pressure-sensitive paint under low-pressure conditions," *Measurement Science and Technology,* vol. 34, no. 7, p. 075103, 2023.

[37] Y. Sugioka, D. Numata, K. Asai, S. Koike, K. Nakakita and T. Nakajima, "Polymer/ceramic pressure-sensitive paint with reduced roughness for unsteady measurement in transonic flow," *AIAA Journal,* vol. 56, no. 6, pp. 2145-2156, 2018.

[38] T. Shigeta, T. Nagata, T. Nonomura and K. Asai, "Enhancement of the signal-to-noise ratio of schlieren visualization measurements in low-density wind tunnel tests using modal decomposition," *Journal of Visualization,* vol. 25, pp. 697-712, 2022.

[39] L. A. Young, P. Lee, G. Briggs and E. Aiken, "Mars Rotorcraft: Possibilities, Limitations, and Implications for Human/Robotic Exploration," in IEEE Aerospace Conference, Big Sky, MT, March 2005.

APPENDIX A

The tabulated mean lift and drag coefficients as obtained from the force measurements are presented in this section. The associated standard deviations to the mean values are also presented as are the measured Reynolds and Mach numbers for each angle of attack. Table A.1 and Table A.2 present the force measurements for the clf5605-us-fp and clf5605-jp-f airfoils, respectively. Table A.3 and Table A.4 present the force measurements for the roamx-0201-us-f and roamx-0201-jp-fp airfoils, respectively.

Table A.1. List of C_l and C_d values for clf5605-us-fp with actual *Re* and *M*.

α [deg]	*Re*	*M*	C_l	C_{l_std}	C_d	C_{d_std}
−2.0	20,005	0.607	0.041741	0.001679	0.068803	0.004149
0.0	20,054	0.602	0.247152	0.003250	0.058084	0.004716
0.0 *(repeat)*	19,724	0.601	0.252750	0.004149	0.063273	0.003214
2.0	19,957	0.599	0.422462	0.007880	0.059664	0.004114
2.5	19,964	0.598	0.477280	0.008298	0.062711	0.003280
3.0	19,998	0.602	0.523162	0.010230	0.065789	0.003832
3.5	20,017	0.603	0.567937	0.007862	0.068284	0.004827
4.0	19,965	0.602	0.601181	0.008790	0.070632	0.004621
4.5	19,926	0.600	0.641799	0.010290	0.076203	0.003405
5.0	19,949	0.601	0.681619	0.009926	0.082380	0.003663
5.5	19,867	0.598	0.725006	0.008388	0.089652	0.004416
6.0	19,850	0.600	0.770064	0.010230	0.098460	0.003658
6.0 *(repeat)*	19,750	0.602	0.763214	0.009544	0.099153	0.004316

Table A.2. List of C_l and C_d values for clf5605-jp-f with actual *Re* and *M*.

α [deg]	*Re*	*M*	C_l	C_{l_std}	C_d	C_{d_std}
−2.0	19,959	0.609	0.147123	0.001642	0.073853	0.001829
0.0	19,841	0.606	0.368381	0.006223	0.067625	0.002056
0.0 *(repeat)*	20,038	0.605	0.392968	0.009235	0.062454	0.002231
2.0	19,854	0.607	0.540916	0.007637	0.071504	0.001733
3.0	19,933	0.609	0.632501	0.010257	0.076491	0.002159
4.0	19,827	0.607	0.711044	0.009151	0.083471	0.001496
5.0	19,862	0.609	0.777961	0.008268	0.094723	0.002331
6.0	19,800	0.607	0.854421	0.011096	0.110233	0.003031
6.0 *(repeat)*	19,889	0.599	0.913060	0.010201	0.117307	0.002060

Table A.3. List of C_l and C_d values for roamx-0201-us-f with actual *Re* and *M*.

α [deg]	*Re*	*M*	C_l	C_{l_std}	C_d	C_{d_std}
−2.0	19,986	0.600	-0.008100	0.001721	0.056467	0.002756
0.0	20,060	0.605	0.182051	0.002730	0.045416	0.002001
0.0 *(repeat)*	20,009	0.605	0.162951	0.001501	0.047513	0.001910
2.0	19,965	0.600	0.386695	0.006457	0.043860	0.001987
2.5	19,888	0.598	0.429902	0.006935	0.045571	0.002680
3.0	19,991	0.602	0.478080	0.008471	0.047546	0.001836
3.5	20,026	0.603	0.522944	0.007619	0.049929	0.001813
4.0	19,957	0.601	0.567940	0.007834	0.052459	0.001665
4.5	20,016	0.603	0.637644	0.007894	0.054401	0.002205
5.0	19,946	0.601	0.733680	0.011191	0.060159	0.001863
5.5	19,986	0.601	0.799964	0.015139	0.066739	0.001828
6.0	19,965	0.601	0.860631	0.017826	0.074403	0.002755
6.0 *(repeat)*	19,727	0.593	0.824826	0.017143	0.077271	0.003702

Table A.4. List of C_l and C_d values for roamx-0201-jp-fp with actual *Re* and *M*.

α [deg]	*Re*	*M*	C_l	C_{l_std}	C_d	C_{d_std}
−2.0	20,189	0.603	-0.067870	0.003305	0.060944	0.001440
0.0	20,074	0.598	0.108597	0.000849	0.048828	0.000870
2.0	20,146	0.603	0.296663	0.003713	0.043521	0.001031
3.0	20,064	0.600	0.379755	0.003675	0.046843	0.000815
4.0	20,106	0.601	0.465086	0.006818	0.050899	0.001051
5.0	20,144	0.603	0.545890	0.006819	0.055731	0.001214
6.0	20,174	0.602	0.622021	0.007968	0.061428	0.001125

APPENDIX B

The tabulated mean pressure distribution results are presented in this section. The measured flow conditions for the clf5605-us-fp upper and lower side and presented in Table B.1 and Table B.2, respectively. The measured flow conditions for the roamx-0201-us-pu (upper side) and roamx-0201-us-pl (lower side) models are presented in Table B.3 and Table B.4, respectively. The measured flow conditions for the roamx-0201-jp-fp (upper side only) are presented in Table B.5.The clf5605-us-fp upper and lower side pressure distributions are presented in Table B.6 and Table B.7, respectively. The roamx-0201-us-pu (upper side) and roamx-0201-us-pl (lower side) model pressure distributions are presented Table B.8 and Table B.9, respectively. The roamx-0201-jp-fp upper pressure distributions is presented in Table B.10.

Table B.1. List of actual flow conditions in PSP measurements of clf5605-us-fp (upper side).

α [deg]	*Re*	*M*
−2.0	19,962	0.599
0.0	19,942	0.598
2.0	20,051	0.601
3.0	20,080	0.602
4.0	20,011	0.599
5.0	20,043	0.600
6.0	19,964	0.599

Table B.2. List of actual flow conditions in PSP measurements of clf5605-us-fp (lower side).

α [deg]	*Re*	*M*
−2.0	19,799	0.594
0.0	20,038	0.602
2.0	20,015	0.604
3.0	20,155	0.603
4.0	20,135	0.599
5.0	20,052	0.595
6.0	20,177	0.598

Table B.3. List of actual flow conditions in PSP measurements of roamx-0201-us-pu (upper side).

α [deg]	*Re*	*M*
−2.0	19,868	0.599
0.0	19,850	0.600
2.0	19,936	0.601
3.0	19,963	0.601
4.0	19,903	0.600
5.0	19,987	0.603
6.0	19,898	0.597

Table B.4. List of actual flow conditions in PSP measurements of roamx-0201-us-pl (lower side).

α [deg]	*Re*	*M*
−2.0	19,787	0.593
0.0	19,963	0.597
2.0	19,922	0.598
3.0	19,983	0.600
4.0	20,036	0.600
5.0	20,033	0.601
6.0	19,935	0.597

Table B.5. List of actual flow conditions in PSP measurements of roamx-0201-jp-fp (upper side only).

α [deg]	*Re*	*M*
−2.0	19,932	0.601
0.0	19,965	0.601
2.0	19,865	0.601
3.0	19,929	0.606
4.0	19,817	0.602
5.0	19,973	0.602
6.0	19,869	0.598

Table B.6. Table of C_p value of clf5605-us-fp (upper side).

x/c	$\alpha = -2.0$ [deg]	$\alpha = 0.0$ [deg]	$\alpha = 2.0$ [deg]	$\alpha = 3.0$ [deg]	$\alpha = 4.0$ [deg]	$\alpha = 5.0$ [deg]	$\alpha = 6.0$ [deg]
0	1.182616	0.998129	0.933645	0.588541	0.236759	0.01177	-0.05551
0.01	0.804667	0.560316	0.291025	-0.00751	-0.25735	-0.48937	-0.70104
0.02	0.598053	0.35409	0.040301	-0.19438	-0.40945	-0.62028	-0.83327
0.03	0.451372	0.208983	-0.10438	-0.31224	-0.50894	-0.693	-0.87846
0.04	0.345328	0.11493	-0.20387	-0.39433	-0.56693	-0.73959	-0.90135
0.05	0.263524	0.041761	-0.27403	-0.43709	-0.59277	-0.75721	-0.89864
0.06	0.201369	-0.0165	-0.31605	-0.47545	-0.62234	-0.7584	-0.88252
0.07	0.144318	-0.0623	-0.36042	-0.49679	-0.62851	-0.75979	-0.8636
0.08	0.097403	-0.10098	-0.38762	-0.51787	-0.64059	-0.75587	-0.8393
0.09	0.055088	-0.14051	-0.4146	-0.53745	-0.65286	-0.74814	-0.81675
0.10	0.014352	-0.16978	-0.44144	-0.5476	-0.6566	-0.7401	-0.8016
0.11	-0.01878	-0.20051	-0.45355	-0.56019	-0.65935	-0.73032	-0.77457
0.12	-0.04482	-0.21769	-0.4729	-0.56921	-0.66192	-0.7162	-0.74945
0.13	-0.06898	-0.2354	-0.48094	-0.57174	-0.6577	-0.70057	-0.72814
0.14	-0.0864	-0.24744	-0.48616	-0.56732	-0.64938	-0.68184	-0.70038
0.15	-0.10268	-0.25378	-0.48356	-0.56205	-0.63803	-0.66351	-0.67739
0.16	-0.11288	-0.2605	-0.48593	-0.55653	-0.62443	-0.64556	-0.64397
0.17	-0.12207	-0.26552	-0.47873	-0.54627	-0.6104	-0.61955	-0.62619
0.18	-0.12439	-0.26689	-0.47393	-0.5374	-0.59716	-0.60012	-0.6024
0.19	-0.12676	-0.2605	-0.46377	-0.5293	-0.58235	-0.57743	-0.58007
0.20	-0.12905	-0.26067	-0.44971	-0.50953	-0.56262	-0.55653	-0.56623
0.21	-0.12997	-0.25293	-0.44614	-0.49646	-0.54923	-0.53447	-0.54336
0.22	-0.1345	-0.24871	-0.43777	-0.4897	-0.53808	-0.51896	-0.52628
0.23	-0.13624	-0.25262	-0.42593	-0.47761	-0.51987	-0.50214	-0.50541
0.24	-0.14346	-0.24744	-0.41912	-0.46966	-0.50649	-0.48642	-0.49237
0.25	-0.14691	-0.2499	-0.41521	-0.45494	-0.49716	-0.47049	-0.48467
0.26	-0.15033	-0.25138	-0.4066	-0.44868	-0.47961	-0.45734	-0.47297
0.27	-0.15622	-0.25168	-0.40372	-0.44116	-0.47158	-0.44337	-0.46441
0.28	-0.16078	-0.25109	-0.39953	-0.43786	-0.46436	-0.4337	-0.45142
0.29	-0.16508	-0.25111	-0.39569	-0.42716	-0.44991	-0.42187	-0.44471
0.30	-0.1688	-0.24695	-0.39355	-0.42358	-0.44972	-0.40626	-0.43493
0.31	-0.1727	-0.25008	-0.38783	-0.41325	-0.4344	-0.39839	-0.42868
0.32	-0.17241	-0.24919	-0.37783	-0.40617	-0.42238	-0.38993	-0.41652
0.33	-0.17378	-0.24551	-0.37583	-0.3986	-0.41396	-0.3811	-0.41625
0.34	-0.17281	-0.24465	-0.36871	-0.38982	-0.40454	-0.3703	-0.41622
0.35	-0.1711	-0.24378	-0.36313	-0.38272	-0.39384	-0.36481	-0.40396
0.36	-0.17297	-0.23861	-0.35674	-0.37317	-0.38872	-0.35614	-0.40076
0.37	-0.17228	-0.23542	-0.35027	-0.36661	-0.37929	-0.35143	-0.39606
0.38	-0.17262	-0.23243	-0.34207	-0.35747	-0.36501	-0.34759	-0.39693
0.39	-0.17454	-0.23099	-0.33569	-0.3529	-0.35595	-0.34639	-0.39732
0.40	-0.17254	-0.23032	-0.33459	-0.34808	-0.3494	-0.334	-0.39013
0.41	-0.1725	-0.2244	-0.32571	-0.34111	-0.3412	-0.32945	-0.38412
0.42	-0.17436	-0.22495	-0.3229	-0.33494	-0.33967	-0.32537	-0.38493
0.43	-0.17387	-0.22607	-0.32109	-0.32522	-0.3309	-0.32304	-0.38147
0.44	-0.17299	-0.22301	-0.31494	-0.32197	-0.325	-0.31842	-0.38109
0.45	-0.17095	-0.22092	-0.30434	-0.31614	-0.31866	-0.31696	-0.37847
0.46	-0.17175	-0.22145	-0.30442	-0.30881	-0.30966	-0.31259	-0.37613
0.47	-0.17085	-0.21847	-0.29568	-0.30227	-0.29755	-0.31199	-0.37421
0.48	-0.17165	-0.21511	-0.29161	-0.29675	-0.29885	-0.30853	-0.37145
0.49	-0.17346	-0.21562	-0.28721	-0.29509	-0.29103	-0.30668	-0.37252
0.50	-0.17417	-0.21526	-0.28259	-0.28617	-0.28265	-0.3088	-0.37641
0.51	-0.17408	-0.21441	-0.28048	-0.28229	-0.27284	-0.30533	-0.37579

x/c	$\alpha = -2.0$ [deg]	$\alpha = 0.0$ [deg]	$\alpha = 2.0$ [deg]	$\alpha = 3.0$ [deg]	$\alpha = 4.0$ [deg]	$\alpha = 5.0$ [deg]	$\alpha = 6.0$ [deg]
0.52	-0.17566	-0.21448	-0.28045	-0.27659	-0.26838	-0.30467	-0.37304
0.53	-0.17625	-0.21231	-0.2771	-0.27234	-0.26357	-0.29742	-0.37092
0.54	-0.17633	-0.20912	-0.27106	-0.26803	-0.26234	-0.29903	-0.37725
0.55	-0.17498	-0.20942	-2.66E-01	-0.26378	-0.25535	-0.29789	-0.37062
0.56	-0.17702	-0.20731	-2.65E-01	-0.25544	-0.25444	-0.29795	-0.36821
0.57	-0.17387	-0.20217	-0.26198	-0.25174	-0.25052	-0.29555	-0.36877
0.58	-0.17472	-0.20393	-0.25647	-0.24498	-0.24626	-0.29743	-0.37339
0.59	-0.17531	-0.20274	-0.25071	-0.24306	-0.23934	-0.29593	-0.36877
0.6	-0.17235	-0.20566	-0.24829	-0.24236	-0.23654	-0.29486	-0.36984
0.61	-0.17263	-0.20127	-0.24255	-0.23569	-0.2313	-0.29581	-0.36702
0.62	-0.17042	-0.19765	-0.23988	-0.22969	-0.23039	-0.29244	-0.37256
0.63	-0.17051	-0.19471	-0.23867	-0.22405	-0.22789	-0.29504	-0.37636
0.64	-0.1704	-0.19631	-0.22977	-0.221	-0.22052	-0.29351	-0.37065
0.65	-0.16957	-0.18978	-0.2274	-0.21405	-0.21747	-0.2912	-0.37195
0.66	-0.17012	-0.18835	-0.2217	-0.21501	-0.21381	-0.29277	-0.37188
0.67	-0.16816	-0.18824	-0.22031	-0.21017	-0.21143	-0.29013	-0.37622
0.68	-0.16792	-0.18659	-0.21624	-0.2041	-0.21269	-0.29402	-0.37294
0.69	-0.16729	-0.18013	-0.21364	-0.20165	-0.21137	-0.29164	-0.38013
0.70	-0.16503	-0.17837	-0.20745	-0.19689	-0.20657	-0.29522	-0.3758
0.71	-0.164	-0.17484	-0.20724	-0.1922	-0.2062	-0.29543	-0.37874
0.72	-0.16372	-0.17719	-0.20169	-0.19061	-0.20332	-0.29805	-0.38418
0.73	-0.16251	-0.17384	-0.19814	-0.18783	-0.20493	-0.29625	-0.38804
0.74	-0.15977	-0.17075	-0.19489	-0.18506	-0.1982	-0.29933	-0.38523
0.75	-0.1585	-0.16789	-0.18904	-0.1794	-0.20119	-0.30341	-0.38946
0.76	-0.155	-0.16525	-0.18574	-0.1763	-0.19912	-0.30495	-0.39145
0.77	-0.15202	-0.15936	-0.18281	-0.17536	-0.19895	-0.30506	-0.39907
0.78	-0.14751	-0.15486	-0.17633	-0.17326	-0.19791	-0.31066	-0.40316
0.79	-0.14414	-0.15076	-0.17241	-0.17032	-0.19669	-0.30904	-0.40827
0.80	-0.14051	-0.14989	-0.1686	-0.16902	-0.19609	-0.31347	-0.40268
0.81	-0.13345	-0.14686	-0.16568	-0.16539	-0.19649	-0.31556	-0.40716
0.82	-0.13075	-0.14091	-0.16485	-0.16524	-0.20104	-0.31821	-0.41969
0.83	-0.12581	-0.1369	-0.16046	-0.16479	-0.1968	-0.32126	-0.42106
0.84	-0.12308	-0.13468	-0.15568	-0.16467	-0.19757	-0.32713	-0.42377
0.85	-0.11657	-0.13052	-0.15515	-0.16327	-0.20109	-0.32944	-0.43568
0.86	-0.11444	-0.1307	-0.15325	-0.1642	-0.19944	-0.33261	-0.43761
0.87	-0.11066	-0.12678	-0.15272	-0.16347	-0.20019	-0.34063	-0.44113
0.88	-0.10867	-0.12261	-0.15043	-0.16085	-0.20282	-0.34059	-0.44678
0.89	-0.10499	-0.12368	-0.15182	-0.16346	-0.20584	-0.3506	-0.45492
0.90	-0.10481	-0.12085	-0.15062	-0.16296	-0.20995	-0.35401	-0.46221
0.91	-0.10116	-0.1208	-0.14769	-0.16468	-0.21263	-0.35787	-0.46603
0.92	-0.10102	-0.11857	-0.1495	-0.1676	-0.21654	-0.36794	-0.47084
0.93	-0.10035	-0.11661	-0.15012	-0.17046	-0.21437	-0.37056	-0.47302
0.94	-0.09906	-0.11806	-0.15179	-0.17294	-0.22188	-0.38288	-0.47813
0.95	-0.10044	-0.12002	-0.14891	-0.17389	-0.22793	-0.38969	-0.48266
0.96	-0.10063	-0.11684	-0.15473	-0.18349	-0.2277	-0.39819	-0.48575
0.97	-0.1023	-0.1175	-0.15474	-0.18291	-0.2308	-0.40658	-0.48232
0.98	-0.10294	-0.11905	-0.16158	-0.18696	-0.23807	-0.41492	-0.48027
0.99	-0.1046	-0.11382	-0.17069	-0.18905	-0.24039	-0.41661	-0.48179
1.00	-0.12214	-0.10932	-0.17141	-0.19096	-0.19839	-0.38008	-0.42585

Table B.7. Table of C_p value of clf5605-us-fp (lower side).

x/c	$\alpha = -2.0$ [deg]	$\alpha = 0.0$ [deg]	$\alpha = 2.0$ [deg]	$\alpha = 3.0$ [deg]	$\alpha = 4.0$ [deg]	$\alpha = 5.0$ [deg]	$\alpha = 6.0$ [deg]
0	-0.71886	-0.79992	-0.70852	-0.94286	-0.54303	0.029837	0.202552
0.01	-0.8996	-0.90288	-0.92922	-0.63631	-0.44716	-0.09445	0.079211
0.02	-0.805	-0.75458	-0.75489	-0.53972	-0.38431	-0.11934	0.020068
0.03	-0.77198	-0.68919	-0.65372	-0.45857	-0.34705	-0.11648	0.007206
0.04	-0.75702	-0.65842	-0.58468	-0.39243	-0.29698	-0.08869	0.018812
0.05	-0.74934	-0.63846	-0.53286	-0.34206	-0.2517	-0.06572	0.030642
0.06	-0.7434	-0.62561	-0.49412	-0.30617	-0.22096	-0.04925	0.038419
0.07	-0.73971	-0.61616	-0.46397	-0.27444	-0.19251	-0.03694	0.044002
0.08	-0.73779	-0.60773	-0.43935	-0.24678	-0.17186	-0.0262	0.045541
0.09	-0.739	-0.60395	-0.41857	-0.22238	-0.15436	-0.01812	0.048002
0.10	-0.7345	-0.59898	-0.39596	-0.2032	-0.13985	-0.01316	0.050264
0.11	-0.73147	-0.59516	-0.37983	-0.18402	-0.12682	-0.00561	0.053081
0.12	-0.73438	-0.59218	-0.36296	-0.16646	-0.11363	0.000211	0.057162
0.13	-0.73281	-0.59075	-0.3498	-0.15635	-0.10606	0.005213	0.056177
0.14	-0.72987	-0.58818	-0.33881	-0.14436	-0.09253	0.008333	0.059871
0.15	-0.73295	-0.5862	-0.329	-0.12583	-0.08363	0.017379	0.0641
0.16	-0.73342	-0.5822	-0.31791	-0.11555	-0.0745	0.023443	0.068005
0.17	-0.7331	-0.5784	-0.3057	-0.10384	-0.06495	0.031059	0.06958
0.18	-0.73409	-0.5799	-0.29773	-0.09115	-0.05538	0.03347	0.075759
0.19	-0.73724	-0.58164	-0.29195	-0.07898	-0.04845	0.039688	0.080469
0.20	-0.74207	-0.5804	-0.28431	-0.06927	-0.03836	0.047311	0.083904
0.21	-0.74164	-0.58131	-0.27786	-0.06331	-0.03035	0.054581	0.090198
0.22	-0.74423	-0.5888	-0.27194	-0.05377	-0.02201	0.063116	0.095897
0.23	-0.74561	-0.5861	-0.26481	-0.04182	-0.01525	0.068207	0.099184
0.24	-0.74504	-0.59375	-0.26198	-0.0369	-0.00766	0.070911	0.104512
0.25	-0.75071	-0.59358	-0.25636	-0.03127	0.00122	0.077657	0.10768
0.26	-0.74891	-0.59731	-0.25172	-0.02265	0.005752	0.08179	0.112663
0.27	-0.75404	-0.59929	-0.24899	-0.01995	0.015493	0.088021	0.115855
0.28	-0.74981	-0.60289	-0.24435	-0.01114	0.020801	0.092192	0.119457
0.29	-0.74784	-0.59599	-0.24206	-0.00561	0.022904	0.095903	0.120575
0.30	-0.74443	-0.5973	-0.23761	0.001317	0.028278	0.099289	0.123007
0.31	-0.73895	-0.59355	-0.23671	0.007775	0.034205	0.101611	0.126493
0.32	-0.7321	-0.58672	-0.23158	0.010023	0.037416	0.104137	0.128036
0.33	-0.72291	-0.58063	-0.23019	0.013823	0.042182	0.10983	0.130747
0.34	-0.70878	-0.56239	-0.23031	0.020549	0.047772	0.112847	0.134631
0.35	-0.70063	-0.54555	-0.2288	0.027247	0.052782	0.117731	0.136657
0.36	-0.68352	-0.52232	-0.22216	0.030581	0.056048	0.118283	0.140034
0.37	-0.66739	-0.49948	-0.22186	0.036508	0.05896	0.12056	0.139568
0.38	-0.65143	-0.46805	-0.21867	0.039012	0.061339	0.121002	0.142027
0.39	-0.63166	-0.44448	-0.22105	0.041826	0.068036	0.129318	0.140705
0.40	-0.61438	-0.41713	-0.21515	0.042847	0.067688	0.127165	0.139722
0.41	-0.59911	-0.38575	-0.21391	0.050507	0.073329	0.130809	0.146293
0.42	-0.58106	-0.35707	-0.20855	0.052292	0.077162	0.13547	0.149379
0.43	-0.56332	-0.32321	-0.20119	0.057774	0.07905	0.13599	0.15015
0.44	-0.54773	-0.29169	-0.19364	0.064542	0.082518	0.136408	0.151618
0.45	-0.52735	-0.27139	-0.18752	0.066225	0.084885	0.140736	0.153214
0.46	-0.50419	-0.24294	-0.17737	0.064052	0.089498	0.143264	0.153292
0.47	-0.48538	-0.21967	-0.16529	0.061418	0.087963	0.143326	0.153568
0.48	-0.4723	-0.19778	-0.15619	0.071627	0.095787	0.14929	0.160733
0.49	-0.46009	-0.18281	-0.14456	0.073841	0.097933	0.149112	0.159741
0.50	-0.43985	-0.15538	-0.12864	0.076785	0.100909	0.15254	0.163266
0.51	-0.42897	-0.14117	-0.11399	0.084702	0.104152	0.15604	0.164911

x/c	$\alpha = -2.0$ [deg]	$\alpha = 0.0$ [deg]	$\alpha = 2.0$ [deg]	$\alpha = 3.0$ [deg]	$\alpha = 4.0$ [deg]	$\alpha = 5.0$ [deg]	$\alpha = 6.0$ [deg]
0.52	-0.41035	-0.12506	-0.09846	0.082199	0.102678	0.159743	0.167253
0.53	-0.39526	-0.10575	-0.08078	0.084662	0.105544	0.156846	0.165991
0.54	-0.38017	-0.09565	-0.0633	0.088906	0.110007	0.160244	0.168909
0.55	-0.36573	-0.07849	-4.61E-02	0.091368	0.112908	0.165138	0.172717
0.56	-0.35494	-0.07033	-2.96E-02	0.096284	0.114922	0.16601	0.174622
0.57	-0.34072	-0.0611	-0.0148	0.093096	0.117776	0.16648	0.177475
0.58	-0.32883	-0.05199	-0.00297	0.093531	0.124396	0.1722	0.180726
0.59	-0.32098	-0.04417	0.013787	0.098487	0.120996	0.170683	0.17986
0.6	-0.30534	-0.03577	0.026866	0.1007	0.124608	0.176742	0.182439
0.61	-0.29458	-0.02914	0.038941	0.104339	0.128242	0.173854	0.182873
0.62	-0.28672	-0.01772	0.05099	0.110917	0.130862	0.175643	0.184769
0.63	-0.27761	-0.01239	0.060962	0.109005	0.133716	0.177618	0.184268
0.64	-0.26462	-0.01343	0.071418	0.108353	0.138973	0.181674	0.18919
0.65	-0.2549	-0.00485	0.078743	0.108734	0.135272	0.182176	0.186876
0.66	-0.24604	-0.00295	0.087879	0.116913	0.136755	0.18742	0.190603
0.67	-0.24379	0.002167	0.091134	0.118999	0.138972	0.185387	0.190657
0.68	-0.23298	0.003441	0.097736	0.112761	0.14005	0.185035	0.191309
0.69	-0.22763	0.006835	0.100073	0.115521	0.1421	0.192351	0.19177
0.70	-0.22324	0.009064	0.105317	0.118882	0.14095	0.187882	0.192637
0.71	-0.21228	0.0088	0.109671	0.114732	0.145083	0.188134	0.189807
0.72	-0.20963	0.016628	0.114041	0.119953	0.147998	0.192199	0.196731
0.73	-0.20056	0.020035	0.115362	0.118736	0.145974	0.190224	0.19333
0.74	-0.19527	0.024633	0.119031	0.126251	0.144858	0.192421	0.193919
0.75	-0.18921	0.027743	0.121683	0.121301	0.149465	0.19336	0.194317
0.76	-0.18502	0.027555	0.123695	0.12508	0.15072	0.193936	0.193394
0.77	-0.17515	0.028604	0.124573	0.130368	0.150342	0.195943	0.197765
0.78	-0.17813	0.029066	0.126067	0.126733	0.151401	0.194082	0.192541
0.79	-0.16994	0.031163	0.126926	0.130912	0.152418	0.19207	0.192469
0.80	-0.16704	0.030689	0.125871	0.134551	0.153741	0.19658	0.192528
0.81	-0.16797	0.031222	0.12404	0.129196	0.147198	0.190223	0.186412
0.82	-0.16221	0.029525	0.124093	0.13368	0.154185	0.191046	0.185764
0.83	-0.15878	0.027044	0.121729	0.130501	0.153925	0.187978	0.186223
0.84	-0.15381	0.028795	0.118964	0.126837	0.150002	0.187886	0.18269
0.85	-0.15676	0.025177	0.116992	0.128263	0.150677	0.187722	0.179899
0.86	-0.15369	0.023906	0.113149	0.130183	0.14689	0.186275	0.174548
0.87	-0.15014	0.021752	0.108777	0.126729	0.141378	0.178951	0.170247
0.88	-0.15028	0.018311	0.103243	0.125291	0.140337	0.173533	0.160762
0.89	-0.14825	0.014117	0.100577	0.126816	0.136046	0.166681	0.151941
0.90	-0.14769	0.010886	0.093593	0.123004	0.136117	0.159458	0.144174
0.91	-0.15071	0.00773	0.089496	0.111155	0.122194	0.156481	0.136237
0.92	-0.14871	0.006991	0.087804	0.108287	0.120377	0.147608	0.128008
0.93	-0.14937	0.000303	0.082505	0.096122	0.110893	0.142258	0.119175
0.94	-0.15133	-0.00684	0.075063	0.090071	0.104011	0.132915	0.108342
0.95	-0.16142	-0.01483	0.059568	0.082666	0.086998	0.114928	0.088751
0.96	-0.16391	-0.03167	0.042368	0.062961	0.068391	0.093849	0.065755
0.97	-0.17523	-0.05284	0.016361	0.034585	0.039567	0.068625	0.03465
0.98	-0.19168	-0.08441	-0.0254	-0.0028	-0.00325	0.023421	-0.01555
0.99	-0.21499	-0.12276	-0.07436	-0.07218	-0.07667	-0.02509	-0.06971
1.00	-0.3101	-0.24646	-0.22883	-0.213	-0.23639	-0.15444	-0.22015

Table B.8. Table of C_p value of roamx-0201-us-pu (upper side).

x/c	$\alpha = -2.0$ [deg]	$\alpha = 0.0$ [deg]	$\alpha = 2.0$ [deg]	$\alpha = 3.0$ [deg]	$\alpha = 4.0$ [deg]	$\alpha = 5.0$ [deg]	$\alpha = 6.0$ [deg]
0	0.933938	0.470577	0.166038	0.22008	-0.28026	0.087274	-0.63611
0.01	0.555968	0.280264	-0.20875	-0.54095	-0.96284	-1.28541	-1.23649
0.02	0.53247	0.315485	-0.07593	-0.32718	-0.70809	-0.97801	-1.06295
0.03	0.499852	0.314766	-0.01766	-0.22216	-0.57682	-0.86265	-0.99573
0.04	0.468216	0.303594	0.009795	-0.1603	-0.48577	-0.78557	-0.95734
0.05	0.438517	0.288375	0.02098	-0.12244	-0.41684	-0.73221	-0.92913
0.06	0.407776	0.268193	0.018477	-0.10204	-0.36444	-0.68326	-0.90447
0.07	0.377677	0.24645	0.012328	-0.0926	-0.32384	-0.63834	-0.88551
0.08	0.350206	0.226391	0.003889	-0.08918	-0.29302	-0.59603	-0.86885
0.09	0.329769	0.211419	-0.00366	-0.08624	-0.26885	-0.55809	-0.85293
0.10	0.305788	0.192194	-0.01359	-0.08938	-0.25372	-0.52288	-0.8387
0.11	0.281581	0.174233	-0.0247	-0.09601	-0.24112	-0.48841	-0.82381
0.12	0.262101	0.156791	-0.03432	-0.10084	-0.23454	-0.45655	-0.81253
0.13	0.245108	0.144487	-0.04189	-0.10702	-0.22984	-0.42553	-0.80046
0.14	0.225604	0.127972	-0.05331	-0.11202	-0.22599	-0.39805	-0.79141
0.15	0.20963	0.115198	-0.06074	-0.11789	-0.22693	-0.37186	-0.77887
0.16	0.191655	0.099916	-0.06946	-0.12358	-0.22703	-0.34689	-0.77106
0.17	0.175812	0.08777	-0.07808	-0.1286	-0.22946	-0.3268	-0.7603
0.18	0.162304	0.079593	-0.08432	-0.13188	-0.2268	-0.30728	-0.75145
0.19	0.14829	0.068301	-0.08879	-0.13364	-0.22639	-0.28821	-0.74143
0.20	0.13523	0.057229	-0.09516	-0.14085	-0.22943	-0.27344	-0.73358
0.21	0.123461	0.048602	-0.09981	-0.14295	-0.2296	-0.26115	-0.72342
0.22	0.112924	0.040788	-0.10358	-0.14269	-0.2276	-0.2458	-0.7144
0.23	0.101461	0.030112	-0.1092	-0.14545	-0.22874	-0.23648	-0.70559
0.24	0.090246	0.022643	-0.11288	-0.1508	-0.22918	-0.2272	-0.69848
0.25	0.078177	0.012674	-0.12053	-0.15256	-0.22879	-0.21924	-0.68747
0.26	0.070827	0.007673	-0.12086	-0.15339	-0.22827	-0.21059	-0.68007
0.27	0.060624	0.000122	-0.12579	-0.15517	-0.22674	-0.20453	-0.66882
0.28	0.048993	-0.00791	-0.12995	-0.15837	-0.22742	-0.20055	-0.65692
0.29	0.039477	-0.0167	-0.13447	-0.16232	-0.22963	-0.19628	-0.64605
0.30	0.030488	-0.02245	-0.13928	-0.16481	-0.22919	-0.19287	-0.63066
0.31	0.024217	-0.02638	-0.14011	-0.163	-0.22702	-0.18876	-0.61641
0.32	0.014757	-0.03442	-0.14374	-0.16553	-0.228	-0.18595	-0.59886
0.33	0.006612	-0.04097	-0.14994	-0.17018	-0.22867	-0.18212	-0.57977
0.34	-0.00185	-0.04668	-0.15318	-0.17282	-0.22722	-0.1825	-0.55724
0.35	-0.00783	-0.05057	-0.15517	-0.17373	-0.22742	-0.1793	-0.53412
0.36	-0.01286	-0.05347	-0.15912	-0.17233	-0.226	-0.17601	-0.50958
0.37	-0.0201	-0.06048	-0.16078	-0.17557	-0.22612	-0.17484	-0.48096
0.38	-0.02327	-0.06087	-0.16275	-0.17641	-0.22547	-0.171	-0.45441
0.39	-0.02808	-0.06568	-0.16382	-0.17623	-0.22296	-0.16919	-0.43127
0.40	-0.03348	-0.06872	-0.16704	-0.17452	-0.22107	-0.16767	-0.40594
0.41	-0.03901	-0.07328	-0.17063	-0.17747	-0.2201	-0.16615	-0.38294
0.42	-0.0448	-0.07539	-0.17117	-0.17842	-0.21956	-0.16322	-0.36145
0.43	-0.04885	-0.07694	-0.17238	-0.17781	-0.21716	-0.1597	-0.34088
0.44	-0.05297	-0.08012	-0.17313	-0.17713	-0.21376	-0.15869	-0.32093
0.45	-0.05594	-0.08269	-0.1742	-0.17519	-0.21269	-0.15545	-0.30315
0.46	-0.05644	-0.08201	-0.17288	-0.1762	-0.21074	-0.15314	-0.28752
0.47	-0.06075	-0.08323	-0.17365	-0.17264	-0.20407	-0.14709	-0.27221
0.48	-0.06299	-0.08307	-0.17203	-0.17128	-0.20161	-0.14453	-0.26068
0.49	-0.06312	-0.08276	-0.17099	-0.17105	-0.19834	-0.13969	-0.24981
0.50	-0.06307	-0.08191	-0.16672	-0.16571	-0.19423	-0.13296	-0.23816
0.51	-0.06106	-0.08007	-0.16647	-0.16203	-0.18904	-0.13046	-0.22753

x/c	$\alpha = -2.0$ [deg]	$\alpha = 0.0$ [deg]	$\alpha = 2.0$ [deg]	$\alpha = 3.0$ [deg]	$\alpha = 4.0$ [deg]	$\alpha = 5.0$ [deg]	$\alpha = 6.0$ [deg]
0.52	-0.06616	-0.0807	-0.16518	-0.15944	-0.1847	-0.12517	-0.21822
0.53	-0.07233	-0.08391	-0.16633	-0.16133	-0.18159	-0.12117	-0.21203
0.54	-0.07511	-0.08704	-0.16527	-0.16064	-0.17963	-0.11808	-0.2093
0.55	-0.07644	-0.0887	-1.68E-01	-0.15679	-0.17691	-0.11712	-0.20571
0.56	-0.07887	-0.09006	-1.66E-01	-0.15691	-0.17206	-0.11125	-0.20402
0.57	-0.08281	-0.08947	-0.16471	-0.15547	-0.16866	-0.10775	-0.19791
0.58	-0.08296	-0.09032	-0.16394	-0.15353	-0.16456	-0.10354	-0.19496
0.59	-0.08361	-0.08973	-0.16244	-0.14874	-0.16056	-0.0985	-0.19272
0.6	-0.08569	-0.08977	-0.16308	-0.14482	-0.15753	-0.09509	-0.18809
0.61	-0.08833	-0.09157	-0.16021	-0.14394	-0.15193	-0.09054	-0.18408
0.62	-0.08725	-0.08832	-0.15543	-0.14008	-0.1463	-0.08687	-0.18202
0.63	-0.08525	-0.08502	-0.1502	-0.1337	-0.14251	-0.07911	-0.17752
0.64	-0.08504	-0.08383	-0.1489	-0.1299	-0.13743	-0.07636	-0.17069
0.65	-0.086	-0.08146	-0.14543	-0.12643	-0.13255	-0.06842	-0.16561
0.66	-0.08389	-0.07901	-0.14147	-0.12009	-0.12657	-0.06398	-0.16051
0.67	-0.08213	-0.0753	-0.13334	-0.11687	-0.12166	-0.05753	-0.15522
0.68	-0.08118	-0.06991	-0.13058	-0.11203	-0.11621	-0.05389	-0.15074
0.69	-0.07662	-0.07015	-0.12446	-0.10739	-0.11071	-0.04745	-0.14658
0.70	-0.07317	-0.06445	-0.12257	-0.10283	-0.10586	-0.04011	-0.13787
0.71	-0.06794	-0.06203	-0.11439	-0.09453	-0.09968	-0.03744	-0.13037
0.72	-0.06845	-0.05741	-0.11184	-0.08881	-0.09453	-0.03107	-0.12302
0.73	-0.06408	-0.05081	-0.10203	-0.0838	-0.09119	-0.02549	-0.11509
0.74	-0.05948	-0.04693	-0.10156	-0.07878	-0.08409	-0.01971	-0.10617
0.75	-0.05327	-0.04293	-0.09197	-0.07533	-0.0801	-0.01735	-0.09818
0.76	-0.04834	-0.03636	-0.09107	-0.07086	-0.0752	-0.01471	-0.09366
0.77	-0.04397	-0.02999	-0.08246	-0.06616	-0.07293	-0.00814	-0.08229
0.78	-0.03985	-0.02747	-0.07793	-0.05925	-0.06783	-0.00418	-0.07312
0.79	-0.03385	-0.02127	-0.07277	-0.05405	-0.06262	-0.00349	-0.06468
0.80	-0.02835	-0.01654	-0.06788	-0.05018	-0.06299	0.002711	-0.0547
0.81	-0.02143	-0.01099	-0.06304	-0.04599	-0.0582	0.005879	-0.0433
0.82	-0.01754	-0.00667	-0.0599	-0.04261	-0.05707	0.008348	-0.03377
0.83	-0.0148	-0.00027	-0.0518	-0.03988	-0.05357	0.01112	-0.02263
0.84	-0.00389	0.002753	-0.05108	-0.03782	-0.05129	0.016141	-0.01297
0.85	0.000174	0.008228	-0.04613	-0.0339	-0.05108	0.018205	-0.00387
0.86	0.003311	0.011544	-0.04298	-0.03172	-0.04611	0.017708	0.009146
0.87	0.008407	0.01636	-0.0406	-0.02923	-0.04671	0.020698	0.021625
0.88	0.011989	0.020412	-0.03798	-0.02628	-0.04563	0.021199	0.030285
0.89	0.014937	0.020996	-0.03862	-0.0243	-0.04215	0.02105	0.04219
0.90	0.019374	0.026001	-0.0325	-0.02311	-0.04308	0.021801	0.053357
0.91	0.025935	0.028097	-0.03004	-0.02289	-0.04073	0.021387	0.063365
0.92	0.02819	0.030036	-0.02916	-0.02033	-0.04107	0.026687	0.074978
0.93	0.028538	0.033276	-0.03171	-0.02001	-0.04176	0.02576	0.084494
0.94	0.031705	0.034579	-0.02776	-0.01924	-0.04369	0.024293	0.094957
0.95	0.032082	0.03364	-0.02814	-0.01921	-0.04453	0.027099	0.108387
0.96	0.032206	0.036425	-0.03179	-0.0192	-0.04318	0.027374	0.120031
0.97	0.034908	0.037765	-0.03024	-0.02094	-0.04668	0.031804	0.129742
0.98	0.034015	0.036125	-0.02686	-0.02109	-0.04897	0.03487	0.139483
0.99	0.032955	0.037192	-0.02991	-0.02224	-0.05624	0.043341	0.148811
1.00	-0.14599	0.016814	-1.46654	-0.21958	-0.36049	0.392946	0.246534

Table B.9. Table of C_p value of roamx-0201-us-pl (lower side).

x/c	$\alpha = -2.0$ [deg]	$\alpha = 0.0$ [deg]	$\alpha = 2.0$ [deg]	$\alpha = 3.0$ [deg]	$\alpha = 4.0$ [deg]	$\alpha = 5.0$ [deg]	$\alpha = 6.0$ [deg]
0	-0.56687	-0.72286	-0.44669	0.444987	0.411017	0.545395	-0.65582
0.01	-0.32551	-0.466	-0.30948	-0.07755	0.220039	0.304965	0.561877
0.02	-0.25289	-0.28487	-0.14344	0.007214	0.253757	0.293074	0.513868
0.03	-0.22926	-0.21092	-0.06056	0.046651	0.2688	0.285306	0.486372
0.04	-0.21422	-0.16908	-0.01192	0.076973	0.279175	0.285564	0.467908
0.05	-0.20546	-0.13822	0.025555	0.096963	0.28677	0.285014	0.455228
0.06	-0.19798	-0.11523	0.055749	0.110943	0.291637	0.283155	0.446517
0.07	-0.19205	-0.09536	0.080126	0.124577	0.297312	0.284743	0.442488
0.08	-0.18823	-0.08203	0.099023	0.133043	0.301581	0.282618	0.438597
0.09	-0.18388	-0.06894	0.116081	0.144622	0.30964	0.28519	0.431157
0.10	-0.18128	-0.05952	0.130869	0.154304	0.314177	0.286948	0.435089
0.11	-0.17749	-0.05038	0.14494	0.163505	0.319438	0.291439	0.433139
0.12	-0.1767	-0.04308	0.156772	0.171983	0.321415	0.292843	0.435152
0.13	-0.17585	-0.03616	0.167762	0.180286	0.327279	0.297176	0.43449
0.14	-0.17599	-0.03192	0.17941	0.189166	0.332844	0.300147	0.43614
0.15	-0.17632	-0.02918	0.188057	0.19629	0.339903	0.305215	0.43971
0.16	-0.17691	-0.02538	0.19641	0.202902	0.342872	0.30881	0.439635
0.17	-0.17709	-0.02234	0.20625	0.209558	0.347588	0.312573	0.442099
0.18	-0.17956	-0.01986	0.216826	0.217501	0.354079	0.315672	0.441669
0.19	-0.18355	-0.01912	0.221639	0.22311	0.35689	0.31835	0.444495
0.20	-0.1846	-0.01817	0.231196	0.229519	0.362296	0.321183	0.444236
0.21	-0.18786	-0.01733	0.237722	0.235002	0.366371	0.325937	0.444391
0.22	-0.19081	-0.0158	0.244838	0.240143	0.371364	0.328443	0.447905
0.23	-0.19203	-0.01356	0.250359	0.246727	0.37323	0.330304	0.446579
0.24	-0.19016	-0.00872	0.25649	0.250124	0.377986	0.333757	0.448662
0.25	-0.18835	-0.00209	0.261391	0.254974	0.38148	0.337129	0.449872
0.26	-0.184	0.008174	0.266535	0.25876	0.384591	0.339381	0.450802
0.27	-0.17505	0.022065	0.272085	0.2627	0.384969	0.340367	0.450039
0.28	-0.1611	0.041912	0.273624	0.265887	0.386992	0.340122	0.449989
0.29	-0.14492	0.067104	0.281333	0.268898	0.391077	0.343536	0.449001
0.30	-0.12562	0.092085	0.282535	0.27129	0.392837	0.343458	0.450046
0.31	-0.10215	0.11979	0.288228	0.276462	0.395081	0.346562	0.447984
0.32	-0.07813	0.14917	0.291656	0.278001	0.394247	0.345658	0.448172
0.33	-0.05006	0.179783	0.294939	0.28048	0.396712	0.348036	0.444968
0.34	-0.02265	0.207385	0.296086	0.28164	0.398384	0.349212	0.445589
0.35	0.006261	0.23183	0.299937	0.284276	0.400978	0.350423	0.441573
0.36	0.033739	0.256302	0.301708	0.286459	0.40198	0.3488	0.44204
0.37	0.059682	0.275814	0.30471	0.287424	0.402266	0.348595	0.43959
0.38	0.085202	0.295401	0.306049	0.289876	0.401566	0.351208	0.439626
0.39	0.109223	0.309421	0.308566	0.291055	0.40351	0.350286	0.438505
0.40	0.133635	0.321498	0.309951	0.291784	0.405104	0.350757	0.438718
0.41	0.155116	0.330916	0.311323	0.293093	0.405245	0.350955	0.43646
0.42	0.175065	0.339379	0.313415	0.294552	0.406358	0.35183	0.43412
0.43	0.194518	0.346816	0.314097	0.295764	0.404546	0.350432	0.435924
0.44	0.210787	0.351785	0.317286	0.297925	0.407189	0.350922	0.431798
0.45	0.222852	0.356543	0.318205	0.2984	0.407282	0.351738	0.432317
0.46	0.239277	0.36298	0.32178	0.299612	0.408906	0.352659	0.430176
0.47	0.250346	0.369529	0.322594	0.300179	0.409095	0.353175	0.430935
0.48	0.262964	0.371595	0.32335	0.301296	0.410058	0.352876	0.430755
0.49	0.273835	0.375189	0.326458	0.304926	0.410763	0.353538	0.431714
0.50	0.287673	0.387695	0.331086	0.307922	0.418034	0.360403	0.433445
0.51	0.294529	0.383131	0.329697	0.306993	0.415301	0.357738	0.43069

x/c	$\alpha = -2.0$ [deg]	$\alpha = 0.0$ [deg]	$\alpha = 2.0$ [deg]	$\alpha = 3.0$ [deg]	$\alpha = 4.0$ [deg]	$\alpha = 5.0$ [deg]	$\alpha = 6.0$ [deg]
0.52	0.301202	0.379836	0.330769	0.30738	0.413476	0.35576	0.431119
0.53	0.306815	0.379301	0.328772	0.304498	0.414479	0.354237	0.426767
0.54	0.313715	0.379068	0.32982	0.305439	0.408984	0.350433	0.424966
0.55	0.32075	0.380409	3.28E-01	0.303592	0.410195	0.350722	0.423483
0.56	0.324315	0.379466	3.30E-01	0.304224	0.409097	0.347549	0.421936
0.57	0.330505	0.379468	0.327323	0.302555	0.407987	0.345861	0.42065
0.58	0.331929	0.378062	0.325583	0.302128	0.406315	0.342158	0.418886
0.59	0.337214	0.379741	0.326771	0.302183	0.405002	0.340248	0.413733
0.6	0.341019	0.380012	0.32732	0.30113	0.404307	0.339642	0.415019
0.61	0.342076	0.377921	0.32709	0.300735	0.401566	0.336468	0.4129
0.62	0.345412	0.378554	0.32486	0.298301	0.397913	0.335807	0.415062
0.63	0.348913	0.379676	0.324248	0.297978	0.396828	0.332626	0.411919
0.64	0.349999	0.378418	0.32449	0.297827	0.399242	0.332688	0.409685
0.65	0.352483	0.377458	0.325177	0.296949	0.395795	0.329297	0.407173
0.66	0.354278	0.379953	0.323297	0.294876	0.395085	0.3279	0.407354
0.67	0.355389	0.376567	0.321736	0.295338	0.390858	0.326187	0.403579
0.68	0.355868	0.376406	0.320641	0.292499	0.390105	0.323276	0.399339
0.69	0.35498	0.37262	0.319147	0.291005	0.385531	0.317973	0.400851
0.70	0.356674	0.373415	0.316081	0.288843	0.383091	0.312909	0.397721
0.71	0.356851	0.372372	0.313196	0.285609	0.38239	0.311849	0.392603
0.72	0.356517	0.369753	0.314452	0.283096	0.377134	0.307227	0.39441
0.73	0.354373	0.367948	0.307133	0.27881	0.374647	0.305233	0.391165
0.74	0.355877	0.366243	0.306825	0.277323	0.371496	0.298795	0.387512
0.75	0.354325	0.36279	0.304951	0.274198	0.365336	0.296471	0.38195
0.76	0.351187	0.358101	0.298368	0.269172	0.359467	0.289479	0.380096
0.77	0.34947	0.355138	0.293717	0.264287	0.35397	0.281509	0.376011
0.78	0.34616	0.350218	0.290637	0.257764	0.348684	0.275163	0.36667
0.79	0.341257	0.345413	0.28492	0.25291	0.342324	0.268429	0.364059
0.80	0.336836	0.338065	0.278859	0.245542	0.334459	0.258339	0.352344
0.81	0.33266	0.332095	0.272887	0.237635	0.32499	0.248099	0.349262
0.82	0.326758	0.321824	0.266429	0.231172	0.317184	0.239166	0.343442
0.83	0.321362	0.31604	0.257564	0.2197	0.306532	0.230673	0.334853
0.84	0.315524	0.308806	0.245681	0.210515	0.29335	0.218239	0.328187
0.85	0.309185	0.29897	0.237016	0.200045	0.2856	0.205721	0.308048
0.86	0.300585	0.286825	0.225816	0.18808	0.274679	0.192619	0.299623
0.87	0.292321	0.276832	0.212318	0.175257	0.257064	0.176886	0.286435
0.88	0.281856	0.263589	0.196494	0.157841	0.241662	0.157445	0.277006
0.89	0.272147	0.251164	0.18636	0.143884	0.2254	0.14155	0.261116
0.90	0.261791	0.237148	0.170286	0.12801	0.207158	0.123613	0.242002
0.91	0.246767	0.218323	0.146835	0.108264	0.189171	0.096626	0.21751
0.92	0.231374	0.197121	0.127448	0.085697	0.164084	0.07021	0.204547
0.93	0.214073	0.17535	0.100982	0.0614	0.134443	0.044257	0.182449
0.94	0.197744	0.15064	0.075628	0.032383	0.106698	0.011053	0.149196
0.95	0.170822	0.118589	0.035176	-0.00297	0.070296	-0.03551	0.117888
0.96	0.138903	0.072421	-0.00212	-0.05015	0.019594	-0.08581	0.076775
0.97	0.098292	0.014714	-0.05276	-0.10772	-0.04808	-0.15722	0.017745
0.98	0.03538	-0.07313	-0.1331	-0.18827	-0.13181	-0.26014	-0.05964
0.99	0.007893	-0.11108	-0.15963	-0.1954	-0.2072	-0.32781	-0.10639
1.00	1.383287	-0.23542	0.332199	0.568589	-1.06768	-0.47177	-0.93158

Table B.10. Table of C_p value of roamx-0201-jp-fp (upper side).

x/c	$\alpha = -2.0$ [deg]	$\alpha = 0.0$ [deg]	$\alpha = 2.0$ [deg]	$\alpha = 3.0$ [deg]	$\alpha = 4.0$ [deg]	$\alpha = 5.0$ [deg]	$\alpha = 6.0$ [deg]
0	1.71906	1.766259	1.089994	0.579743	0.090637	-0.80435	-0.92184
0.01	0.7747	0.68927	0.322639	0.057299	-0.24841	-0.68054	-0.95713
0.02	0.64064	0.564917	0.26119	0.05429	-0.18624	-0.54046	-0.83961
0.03	0.561015	0.490474	0.223093	0.047999	-0.15551	-0.45186	-0.77162
0.04	0.496702	0.433599	0.189923	0.036871	-0.14155	-0.3948	-0.7246
0.05	0.4405	0.374267	0.148499	0.008053	-0.15182	-0.3622	-0.7004
0.06	0.402837	0.339238	0.125529	-0.00288	-0.14835	-0.33638	-0.66525
0.07	0.358429	0.297595	0.094183	-0.02707	-0.16069	-0.32359	-0.65398
0.08	0.319264	0.261733	0.067174	-0.04829	-0.17244	-0.31631	-0.63962
0.09	0.291009	0.228113	0.04284	-0.06575	-0.18239	-0.31274	-0.62155
0.10	0.262883	0.206537	0.029984	-0.07572	-0.18786	-0.30925	-0.61247
0.11	0.234113	0.179603	0.012128	-0.08869	-0.1947	-0.30895	-0.60727
0.12	0.212855	0.157351	-0.00397	-0.10039	-0.20295	-0.30868	-0.59822
0.13	0.192534	0.139938	-0.01452	-0.10783	-0.20539	-0.30735	-0.59084
0.14	0.171173	0.118498	-0.02968	-0.11949	-0.21355	-0.30853	-0.58441
0.15	0.152097	0.102571	-0.04164	-0.12927	-0.21756	-0.30999	-0.57603
0.16	0.135248	0.082343	-0.05623	-0.14149	-0.22532	-0.31212	-0.56956
0.17	0.116592	0.064535	-0.06772	-0.1483	-0.23136	-0.31236	-0.56437
0.18	0.100653	0.053426	-0.07447	-0.1537	-0.23201	-0.31145	-0.5614
0.19	0.085585	0.040821	-0.08372	-0.16086	-0.23683	-0.31112	-0.55435
0.20	0.072148	0.027278	-0.09118	-0.16615	-0.23997	-0.31271	-0.55295
0.21	0.058928	0.01661	-0.09781	-0.17152	-0.24373	-0.31251	-0.55002
0.22	0.047299	0.005109	-0.10589	-0.17818	-0.24536	-0.31306	-0.54243
0.23	0.0352	-0.0042	-0.11158	-0.18109	-0.2455	-0.31164	-0.5392
0.24	0.02398	-0.01433	-0.11691	-0.18312	-0.24825	-0.3107	-0.53596
0.25	0.013261	-0.02001	-0.1218	-0.18653	-0.24863	-0.30917	-0.53334
0.26	0.004759	-0.02957	-0.1275	-0.18973	-0.24975	-0.30827	-0.52815
0.27	-0.00454	-0.04016	-0.13359	-0.19465	-0.25236	-0.30679	-0.52274
0.28	-0.01396	-0.0437	-0.13646	-0.19959	-0.25392	-0.308	-0.51682
0.29	-0.02085	-0.05525	-0.1405	-0.19832	-0.25285	-0.30327	-0.51715
0.30	-0.02927	-0.06069	-0.14488	-0.1997	-0.25187	-0.30244	-0.50961
0.31	-0.03511	-0.06942	-0.14974	-0.20385	-0.25366	-0.30186	-0.50272
0.32	-0.04381	-0.07189	-0.15112	-0.20459	-0.25213	-0.29714	-0.49416
0.33	-0.05072	-0.07755	-0.15595	-0.20795	-0.25473	-0.29806	-0.48934
0.34	-0.05641	-0.08649	-0.15918	-0.20795	-0.25166	-0.29283	-0.47989
0.35	-0.06159	-0.08731	-0.16326	-0.20909	-0.25234	-0.28945	-0.46538
0.36	-0.06722	-0.09295	-0.16295	-0.21095	-0.25361	-0.29173	-0.4619
0.37	-0.07484	-0.0999	-0.16545	-0.21173	-0.2513	-0.28821	-0.44741
0.38	-0.07802	-0.10164	-0.16782	-0.21234	-0.25002	-0.28652	-0.43885
0.39	-0.08543	-0.10966	-0.16913	-0.21121	-0.25325	-0.28726	-0.42587
0.40	-0.0878	-0.10738	-0.16804	-0.21138	-0.25015	-0.27835	-0.41245
0.41	-0.09558	-0.11562	-0.17597	-0.21208	-0.24958	-0.27561	-0.40155
0.42	-0.1005	-0.11829	-0.17692	-0.21028	-0.24902	-0.27612	-0.39846
0.43	-0.1024	-0.11857	-0.17859	-0.21376	-0.25099	-0.27648	-0.37936
0.44	-0.11216	-0.12308	-0.18183	-0.21714	-0.25138	-0.27356	-0.36673
0.45	-0.12388	-0.13502	-0.18845	-0.21842	-0.24945	-0.26938	-0.35487
0.46	-0.12748	-0.13921	-0.19192	-0.22167	-0.25014	-0.27127	-0.35333
0.47	-0.13196	-0.14078	-0.19449	-0.22356	-0.24873	-0.26835	-0.34456
0.48	-0.13716	-0.14657	-0.19211	-0.22046	-0.24428	-0.2648	-0.32915
0.49	-0.13638	-0.1436	-0.19698	-0.22508	-0.25131	-0.26996	-0.33363
0.50	-0.14001	-0.14789	-0.1924	-0.21707	-0.24065	-0.25711	-0.31861
0.51	-0.14304	-0.14765	-0.1897	-0.21631	-0.23834	-0.25275	-0.3143

x/c	$\alpha = -2.0$ [deg]	$\alpha = 0.0$ [deg]	$\alpha = 2.0$ [deg]	$\alpha = 3.0$ [deg]	$\alpha = 4.0$ [deg]	$\alpha = 5.0$ [deg]	$\alpha = 6.0$ [deg]
0.52	-0.14731	-0.15224	-0.19625	-0.21818	-0.23756	-0.25169	-0.31535
0.53	-0.15215	-0.15568	-0.19589	-0.21738	-0.23726	-0.24796	-0.30848
0.54	-0.15198	-0.15216	-0.19712	-0.21306	-0.23177	-0.24503	-0.30356
0.55	-0.15501	-0.15471	-1.95E-01	-0.21638	-0.2316	-0.23369	-0.29194
0.56	-0.15334	-0.15394	-1.94E-01	-0.20774	-0.22395	-0.23812	-0.29794
0.57	-0.15199	-0.14992	-0.18712	-0.20736	-0.22429	-0.23225	-0.29591
0.58	-0.15024	-0.14866	-0.1835	-0.205	-0.21874	-0.21619	-0.27886
0.59	-0.15032	-0.14661	-0.18218	-0.20019	-0.21143	-0.21099	-0.26834
0.6	-0.15148	-0.14418	-0.17871	-0.19438	-0.208	-0.20605	-0.26622
0.61	-0.15263	-0.14715	-0.17578	-0.19064	-0.20241	-0.20555	-0.26981
0.62	-0.15388	-0.14317	-0.17268	-0.18853	-0.20154	-0.20625	-0.27106
0.63	-0.15229	-0.13755	-0.17189	-0.18207	-0.19588	-0.19869	-0.26413
0.64	-0.15042	-0.13815	-0.16886	-0.17803	-0.18919	-0.19362	-0.25798
0.65	-0.15075	-0.13675	-0.16306	-0.17648	-0.18601	-0.18591	-0.25025
0.66	-0.14957	-0.1341	-0.16213	-0.1706	-0.18005	-0.18158	-0.24392
0.67	-0.14773	-0.13173	-0.15885	-0.165	-0.17554	-0.17933	-0.24355
0.68	-0.14547	-0.12851	-0.15503	-0.16239	-0.16732	-0.17074	-0.23062
0.69	-0.14257	-0.12576	-0.15159	-0.15812	-0.16594	-0.16211	-0.22479
0.70	-0.14154	-0.12183	-0.14467	-0.15213	-0.15815	-0.1566	-0.21704
0.71	-0.13863	-0.11897	-0.1388	-0.14914	-0.15672	-0.15357	-0.21883
0.72	-0.13582	-0.11429	-0.13745	-0.14309	-0.14978	-0.15243	-0.21557
0.73	-0.13379	-0.10984	-0.13187	-0.13768	-0.14735	-0.14913	-0.21214
0.74	-0.12758	-0.1043	-0.12838	-0.1354	-0.14223	-0.14454	-0.20353
0.75	-0.12581	-0.09825	-0.1249	-0.13066	-0.14192	-0.14494	-0.20895
0.76	-0.12119	-0.09438	-0.12052	-0.12702	-0.13717	-0.14203	-0.20005
0.77	-0.11873	-0.09126	-0.11486	-0.12123	-0.12986	-0.13591	-0.19681
0.78	-0.11494	-0.08428	-0.11096	-0.11942	-0.12701	-0.13216	-0.18163
0.79	-0.11025	-0.07997	-0.10776	-0.11291	-0.12549	-0.12951	-0.18151
0.80	-0.1037	-0.0754	-0.10268	-0.11137	-0.12116	-0.12707	-0.17332
0.81	-0.09963	-0.06722	-0.09848	-0.10553	-0.11941	-0.12555	-0.17443
0.82	-0.09321	-0.0648	-0.09417	-0.1047	-0.11824	-0.12583	-0.17053
0.83	-0.09004	-0.06053	-0.09061	-0.1017	-0.11717	-0.12525	-0.16204
0.84	-0.08483	-0.05793	-0.08959	-0.09935	-0.11518	-0.12479	-0.16188
0.85	-0.07834	-0.05075	-0.08424	-0.09756	-0.11216	-0.12268	-0.15744
0.86	-0.07495	-0.05036	-0.08296	-0.09379	-0.11043	-0.12161	-0.15271
0.87	-0.07045	-0.04304	-0.07704	-0.08894	-0.10521	-0.1152	-0.14499
0.88	-0.06558	-0.03774	-0.07526	-0.08682	-0.10475	-0.11224	-0.1448
0.89	-0.06264	-0.03518	-0.07499	-0.08754	-0.10437	-0.11814	-0.1344
0.90	-0.05843	-0.03936	-0.07573	-0.08369	-0.10104	-0.11297	-0.12202
0.91	-0.05825	-0.03291	-0.07234	-0.0888	-0.1034	-0.11873	-0.12888
0.92	-0.05382	-0.0289	-0.07259	-0.08469	-0.10604	-0.11935	-0.13439
0.93	-0.04837	-0.0238	-0.07	-0.09172	-0.11204	-0.12033	-0.1034
0.94	-0.04693	-0.0213	-0.06661	-0.08947	-0.10277	-0.12556	-0.12803
0.95	-0.04524	-0.02231	-0.07225	-0.09236	-0.11481	-0.13011	-0.11549
0.96	-0.04496	-0.02465	-0.07317	-0.09261	-0.11646	-0.12597	-0.10383
0.97	-0.0469	-0.02359	-0.07549	-0.09954	-0.12036	-0.13744	-0.116
0.98	-0.05233	-0.03377	-0.08896	-0.10523	-0.12487	-0.14897	-0.12164
0.99	-0.0564	-0.05024	-0.10832	-0.11874	-0.13512	-0.16144	-0.0961
1.00	-1.45917	-3.61985	-2.47224	-1.43454	-1.59676	-1.23614	-0.61223